HHS Public Access

Author manuscript

Immunity. Author manuscript; available in PMC 2024 April 11.

Published in final edited form as:

Immunity. 2023 April 11; 56(4): 797–812.e4. doi:10.1016/j.immuni.2023.01.023.

Repression of the Aryl Hydrocarbon Receptor Prevents Oxidative Stress and Ferroptosis of Intestinal Intraepithelial Lymphocytes

Santosh K. Panda,

Vincent Peng,

Raki Sudan,

Alina U. Antonova,

Blanda Di Luccia,

Takahiro E. Ohara,

Jose Luis Fachi,

Gary Grajales-Reyes,

Natalia Jaeger,

Tihana Trsan,

Susan Gilfillan,

Marina Cella,

Marco Colonna*

Department of Pathology and Immunology, Washington University School of Medicine, St. Louis, MO 63108, USA.

SUMMARY

The aryl-hydrocarbon receptor (AHR) is a ligand-activated transcription factor that buoys intestinal immune responses. AHR induces its own negative regulator, the AHR repressor (AHRR). Here we show that AHRR is vital to sustain intestinal intraepithelial lymphocytes (IEL). AHRR deficiency reduced IEL representation in a cell-intrinsic fashion. Single-cell RNA-sequencing revealed an oxidative stress profile in *Ahrr*$^{-/-}$ IEL. AHRR deficiency unleashed AHR-induced expression of CYP1A1, a monoxygenase that generates reactive-oxygen species, increasing redox imbalance, lipid peroxidation and ferroptosis in *Ahrr*$^{-/-}$ IEL. Dietary supplementation with selenium or Vitamin-E to restore redox homeostasis rescued *Ahrr*$^{-/-}$ IEL.

*Correspondence: mcolonna@wustl.edu.

AUTHOR CONTRIBUTIONS

SKP, M. Cella and M. Colonna designed the experiments and analyzed the data. SKP, RS, BDL and ZF conducted the experiments. VP and AUA analyzed single cell RNA seq data. SKP, TEO and GGR performed the microscopy. NJ and TT provided the human IBD and healthy patient samples. SG generated mouse colonies and guided animal experiments. SKP wrote the first draft of the manuscript. M. Colonna conceived and directed the study, edited and finalized the manuscript.

DECLARATION OF INTERESTS

Marco Colonna receives research support from Pfizer.

Loss of IEL in *Ahrr*$^{-/-}$ mice caused susceptibility to *Clostridium difficile* infection and dextran sodium sulfate-induced colitis. Inflamed tissue of inflammatory-bowel disease patients showed reduced *Ahrr* expression that may contribute to disease. We conclude that AHR signaling must be tightly regulated to prevent oxidative stress and ferroptosis of IEL and preserve intestinal immune responses.

In Brief

Intestinal IEL homeostasis relies on AHR, a ligand-induced transcription factor that is tightly controlled through feedback circuitries. Panda *et al.* demonstrated that lack of AHR repressor (AHRR) unleashes the AHR-induced monooxygenase CYP1A1, which causes oxidative stress and ferroptosis of IELs. This loss of IELs can be reversed by dietary anti-oxidants.

Graphical Abstract

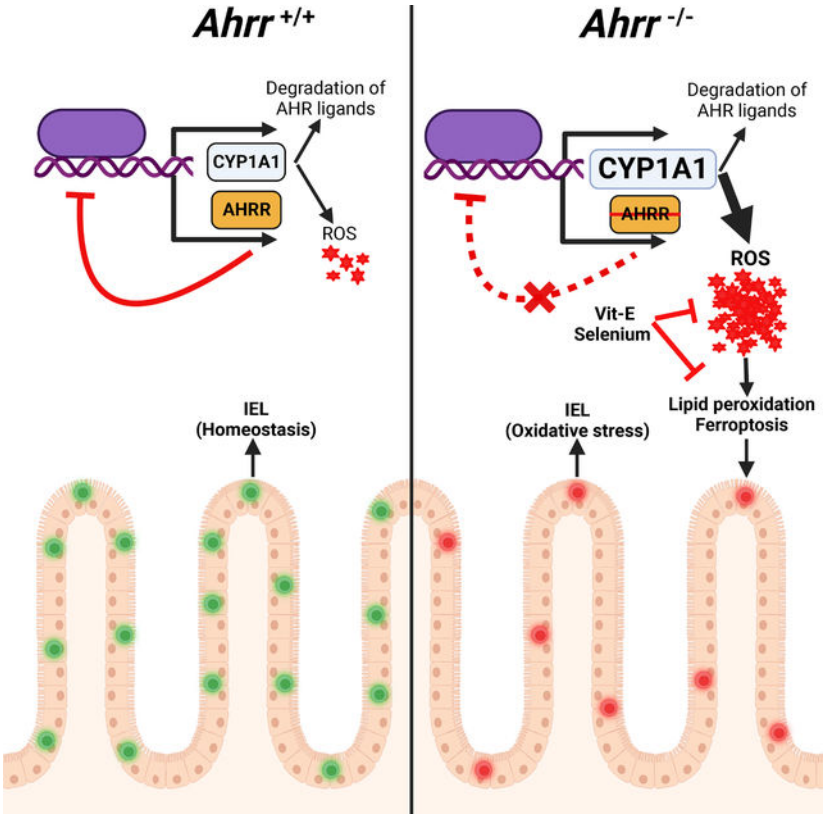

INTRODUCTION

Intestinal intraepithelial lymphocytes (IEL) encompass natural TCRαβ$^+$ CD8αα$^+$ T cells and TCRγδ$^+$ CD8αα$^+$ T cells as well as induced TCRαβ$^+$ CD4$^+$ and TCRαβ$^+$ CD8αβ$^+$ T cells interspersed within intestinal epithelial cells (IEC)[1]. Due to their strategic presence at the interphase between the luminal environment and the intestinal barrier, IEL constantly sense fluctuating environmental components, such as commensal bacteria, pathobionts, pathogens, and dietary components and contribute to maintain the integrity of the intestinal

epithelium in the steady state[2,3]. Moreover, IEL mediate immune responses against various pathogens[4,5] and have protective effects in models of food intolerance and chronic inflammatory bowel disease (IBD)[6]. Mice deficient in IEL are susceptible to both dextran sodium sulfate (DSS)- and T cell-induced colitis[7–9].

The aryl-hydrocarbon receptor (AHR) is a member of basic bHLH-PAS family of transcription factors that promotes gene programs devoted to metabolism of drugs, lipid metabolism, and circadian rhythm. AHR is activated by exogenous and endogenous ligands. Exogenous ligands include environmental toxins, such as 2,3,7,8-Tetrachlorodibenzo-p-dioxin (TCDD)[10,11], dietary derived compounds, such as indole-3-carbinol and its acidic condensation product indolo [3,2-b]carbazole, as well as catabolites of nutritional tryptophan generated by the microbiota[11]. Endogenous ligands include tryptophan metabolites such as kynurenine[12]. Upon ligand binding, AHR translocates into the nucleus and forms a complex with the AHR nuclear translocator (ARNT) that binds to dioxin response element (DRE)-containing genes, inducing their transcription[13]. One of the major effector molecules induced by AHR is the cytochrome P450 family 1 member A1 (CYP1A1), a member of the cytochrome p450 family of monooxygenases[14]. CYP1A1 oxidizes polycyclic aromatic hydrocarbons, often activating their carcinogenic properties[15]. Additionally, it metabolizes polyunsaturated long-chain fatty acids generating several classes of oxygenated metabolites that function as lipid mediators[16]. In the gastrointestinal system, the AHR pathway sustains healthy epithelium, along with the immune system and enteric nervous system. AHR is required for development, maintenance and function of IEL[2,17], as well as the capacity of IEC to maintain barrier functions[18]. AHR is also necessary for the development and function of immune cell types in intestinal lamina propria (LP), including T helper-17 (Th17)[19], regulatory T (Treg)[20], T regulatory 1 (Tr1) cells[21], group 3 innate lymphoid cells (ILC3)[22–24] and group 2 ILC (ILC2)[25], as well as enteric neurons[26]. Downstream of AHR, CYP1A1 also contributes to intestinal homeostasis by metabolizing AHR ligands[27]. Dysregulated CYP1A1 enzymatic activity in IEC degrades dietary and microbial derived AHR ligands, thereby thwarting AHR activation in ILC3 and Th17 cells and undermining their maintenance[27].

In addition to CYP1A1, AHR drives the expression of an AHR repressor (AHRR), which contains both DRE-binding and ARNT-interacting domains but lacks ligand binding and transcription activation domains. Thus, AHRR competes with AHR for ARNT and DRE binding sites, preventing ligand-induced transcriptional activation of genes such as CYP1A1[28,29]. Although AHR is required to maintain intestinal immunity, increased activation of AHR in *Ahrr*$^{-/-}$ mice is paradoxically deleterious. *Ahrr*$^{-/-}$ mice exhibit susceptibility to dextran sulfate sodium (DSS)-induced colitis and reduction of colonic γδ T cells[30]. Why AHRR deficiency affects γδ T cells and, in general, intestinal immunity is unclear. In this study, we found that AHRR deficiency has a broad impact on all IEL, reducing the number of both natural and induced IEL. The deficit of IEL was cell-intrinsic, since IEL were reduced a) after adoptive transfer of *Ahrr*$^{-/-}$ T cells into *Rag1*$^{-/-}$ mice, b) in bone marrow (BM) chimeras created with *Ahrr*$^{-/-}$ BM donors, and c) in mice with a conditional deletion of *Ahrr* gene in T cells. Single-cell RNA-sequencing (scRNA seq) of IEL revealed that AHRR deficiency induced a transcriptional signature indicative of cell stress and exposure to reactive oxygen species (ROS). We further noted

that AHRR deficiency increased the expression and activity of CYP1A1, which produces ROS as a byproduct of its enzymatic activity[31]. We validated more intracellular ROS in *Ahrr*$^{-/-}$ IEL than in WT IEL, which was associated with increased lipid peroxidation and ferroptosis. Dietary supplementation with selenium, an essential element known to contribute to redox homeostasis[32], or Vitamin E (Vit-E), which inhibits ROS, rescued *Ahrr*$^{-/-}$ IEL. The defect of IEL in mice with total or T cell restricted deletion of *Ahrr* increased susceptibility to infection by *Clostridium difficile (C. difficile)* as well as DSS-induced colitis. Taken together, these data reveal that dysregulation of the AHR-CYP1A1 axis due to AHRR deficiency causes excessive ROS generation and ferroptosis in IEL, affecting their maintenance and intestinal resistance to pathogens. Overall, IEL emerge as a T cell subset highly vulnerable to oxidative stress.

RESULTS

Ahrr$^{-/-}$ mice exhibit broad defects in IEL

Since IEL depend on AHR for their maintenance[2], express AHRR[30] and AHRR negatively regulates AHR, we hypothesized that AHRR deficiency may enhance the presence of IEL in the gut. Paradoxically, a marked reduction of intraepithelial T cells in the small intestine was evident in *Ahrr*$^{-/-}$ mice in comparison to wild-type (WT) controls (Figure 1A, B), whereas T cells in LP, mesenteric lymph nodes and spleen remain unaltered numerically (Figure 1C–E). Further, we analyzed various subsets of IEL (Figure S1A) and observed that γδ T (TCR γδ$^+$ CD8αα$^+$) cells, TCRαβ$^+$ CD8αα$^+$, TCRαβ$^+$ CD8αβ$^+$, and TCRαβ$^+$ CD4$^+$ IEL were reduced in the small intestine of *Ahrr*$^{-/-}$ mice in comparison to WT mice (Figure 1F–J). Similarly, total IEL as well as γδ T cells and TCRαβ$^+$ CD4$^+$ IEL were less abundant in the large intestinal epithelium of *Ahrr*$^{-/-}$ mice than WT mice (Figure S1B–G). Staining of CD8α in the ileal tissues confirmed the reduction of IEL in *Ahrr*$^{-/-}$ mice (Figure 1K, L). The receptor CD160 is predominantly expressed by CD8αα$^+$ IEL and triggers IEL functions[3]. Consistent with the CD8αα$^+$ IEL deficit, the frequency of CD160$^+$ CD8αα$^+$ IEL was reduced in *Ahrr*$^{-/-}$ mice (Figure 1M). IEL also include a subset of intraepithelial CD4$^+$ T cells that downregulate the CD4 lineage transcription factor ThPOK, upregulate the CD8 lineage transcription factor Runx3, and express the CD8 cytolytic program[33]. The conversion of CD4$^+$ T cells into CD4$^+$CD8αα$^+$ IEL (which we refer to double positive - DP) depends on AHR[17]. We found that these DP IEL were much less abundant in *Ahrr*$^{-/-}$ mice than in WT mice as assessed by staining for both CD4$^+$CD8αα$^+$ cells (Figure 1N, O) and ThPOK^{lo}CD8αα$^+$ cells (Figure 1P, Q). Since there is regional variation in the distribution of IEL from the proximal to distal small intestine[34], we ascertained whether the impact of *Ahrr* deletion extended along the small intestine or was limited to a specific segment. A progressive decrease of IEL numbers from the proximal to distal intestinal segments was evident in WT mice, with the exception of DP IEL that peaked in the distal intestine. AHRR-deficiency correlated with significantly reduced IEL numbers in the proximal and distal segments, along with a trend towards fewer IEL in the intermediate segment (Figure S1H–N). Thus, AHRR-deficiency affects IEL throughout the small intestine. Further, we examined whether *Ahrr* deletion affects IEL cytokine production. IEL of WT and *Ahrr*$^{-/-}$ mice were isolated from the small intestine, stimulated with immobilized anti-CD3 antibody overnight and analyzed for intracellular content of

IFN-γ by flow cytometry. The percentage of IFN-γ^+ cells was comparable between WT and *Ahrr*$^{-/-}$ IEL (Figure S1O–S), suggesting that AHRR deficiency does not impact the IEL cytokine production on a per cell basis. To investigate whether *Ahrr* gene dosage impacts IEL, we compared IEL subsets in WT and haplo-insufficient *Ahrr*$^{+/-}$ mice. Total CD45$^+$ IEL, TCRαβ$^+$ CD8αα$^+$ IEL, and DP-IEL were reduced in *Ahrr*$^{+/-}$ mice, although other subsets were comparable (Figure S1T–Z), suggesting a partial effect of *Ahrr* gene dosage on IEL.

We further examined the impact of AHRR deficiency on LP lymphocytes which express AHRR[30] and depend on AHR for development and/or function like IEL[10]. Although they express AHRR, ILC3, Th17 and Treg cells in the small intestine lamina propria were similarly represented in WT and *Ahrr*$^{-/-}$ mice (Figure S2A–I). Moreover, production of IL-22 by ILC3 in response to IL-23 was comparable in WT and *Ahrr*$^{-/-}$ mice (Figure S2J–L). *Ahrr* expression in IEL was significantly higher than in lamina propria T cells (Figure S2M), which may in part be the reason why IEL are more vulnerable to AHRR deficiency. The liver does not express AHRR[30]. Accordingly, while mice lacking AHR have hepatic steatosis and reduced body weight[35,36], AHRR deficiency had no impact on liver or body weight (Figure S2N–R). We conclude that *Ahrr* deletion causes a selective reduction of IEL in the steady state. Since AHRR deficiency affected more profoundly small intestine than large intestine IEL, we focused on small intestine IEL for further analysis.

IEL defect in *Ahrr*$^{-/-}$ mice is cell intrinsic

Since AHRR is expressed not only in IEL, but also in intestinal dendritic cells (DC), ILCs and T cells[30], we sought to determine whether the requirement of AHRR for IEL is cell-intrinsic or -extrinsic. To address this question, we co-transferred splenic T cells from WT (CD45.1) and *Ahrr*$^{-/-}$ (CD45.2) mice or WT (CD45.1) and *Ahrr*$^{+/+}$(CD45.2) mice at a 1:1 ratio into *Rag1*$^{-/-}$ recipient mice (Figure 2A). After 8 weeks, T cells from both genotypes had reconstituted the spleen in equal proportions (Figure S3A–C). TCRαβ$^+$ T cells were also detected in the epithelium of the small intestine, as previously reported[37]. The frequency of WT and AHRR sufficient IEL in the epithelium of reconstituted mice were comparable (Figure S3D). However, *Ahrr*$^{-/-}$ T cells were outcompeted by WT T cells in this location: the frequencies and numbers of WT TCRαβ$^+$ CD8αα$^+$, TCRαβ$^+$ CD8αβ$^+$, TCRαβ$^+$ CD4 and DP IEL were significantly higher than their *Ahrr*$^{-/-}$ counterparts (Figure 2B–F, Figure S3E–I), indicating that the impact of AHRR on IEL differentiation or maintenance is cell-intrinsic. Whether the defect of γδ T cells in *Ahrr*$^{-/-}$ is also cell intrinsic could not be determined in this experiment, as we could not recover a sizeable population of γδ T cells from the intestine of adoptively transferred *Rag1*$^{-/-}$ mice.

To corroborate the cell-intrinsic function of AHRR in TCRαβ$^+$ IEL, we crossed *Ahrr*$^{fl/fl}$ mice with *Rorc*^{cre} mice (Figure 2G), such that the *Ahrr* gene is deleted in all T cells as well as ILC3. TCRαβ$^+$ CD8αα$^+$, TCRαβ$^+$ CD8αβ$^+$, TCRαβ$^+$ CD4$^+$ and DP IEL were significantly reduced in *Rorc*^{cre} *Ahrr*$^{fl/fl}$ mice in comparison to *Ahrr*$^{fl/fl}$ mice, corroborating the cell-intrinsic requirement for AHRR in TCRαβ$^+$ IEL development or maintenance (Figure 2H–K). No marked differences were observed in total γδ T cells (Figure 2L). To further confirm the cell-intrinsic function of AHRR, we performed a competitive BM

chimera experiment. Lethally irradiated CD45.1.2 mice were reconstituted with BM cells from WT (CD45.1) and *Ahrr*$^{-/-}$ (CD45.2) mice or, as a control, with WT (CD45.1) and *Ahrr*$^{+/+}$ (CD45.2) mice; all were examined for IEL reconstitution after 8 weeks (Figure 2M). Again, we observed that the frequencies and numbers of *Ahrr*$^{-/-}$ TCRαβ^{+} CD8αα^{+}, TCRαβ^{+} CD8αβ^{+}, TCRαβ^{+} CD4, and DP IEL were significantly lower than their WT IEL counterparts (Figure 2N–R, Figure S3J–N), whereas the frequencies of *Ahrr*$^{+/+}$ CD45.2 IEL and WT IEL were comparable in the control BM chimeras (Figure S3O). Analysis of γδ T cells revealed that *Ahrr* deletion was associated with underrepresentation of Vγ7^{+}δ T cells (Figure 2S, Figure S3P), which are the gut-resident γδ T cell subset[2], whereas circulating γδ T cells were unaffected (Figure S3Q). Altogether, these data corroborate the intrinsic requirement of AHRR for IEL maintenance.

IEL development and homing are AHRR-independent

We asked how AHRR defect impacts intestinal IEL numbers. First, we investigated IEL development and/or migration in *Ahrr*$^{-/-}$ mice. TCRαβ^{+} natural IEL develop from CD4^{-}CD8^{-}NK1.1^{-}TCRαβ^{+}CD5^{+} thymic IEL progenitors (IELp)[38,39], which migrate into the gut and acquire CD8αα expression upon reaching the IL-15-rich intestinal environment. WT and *Ahrr*$^{-/-}$ mice had similar distributions of various CD4- and CD8-expressing thymocyte populations (Figure S4A) and the frequency of thymic IELp was comparable in WT and *Ahrr*$^{-/-}$ mice (Figure S4B, C), indicating that AHRR deficiency does not affect IEL development in thymus. Since differentiation of IEL in the gut requires IL-15 signaling through CD122 (IL2Rβ), we examined expression of CD122 on IELp. Expression of CD122 on the surface of IELp was comparable in WT and *Ahrr*$^{-/-}$ mice (Figure S4D). Moreover, molecules that promote gut homing and tissue retention, such as CCR9, CD103 and CD69[37], were equally expressed in IEL from WT and *Ahrr*$^{-/-}$ mice (Figure S4E–H). Altogether, these data suggest that AHRR deficiency does not affect thymic development or expression of gut homing molecules.

The transcriptional profile of *Ahrr*$^{-/-}$ IEL reveals an oxidative stress response

To further investigate the mechanism by which *Ahrr* deficiency affects IEL numbers in the small intestine, we sorted IEL from WT and *Ahrr*$^{-/-}$ mice and analyzed them by droplet-based 3' single cell RNA sequencing (10X Genomics). Through unsupervised clustering, we identified 14 IEL clusters visualized by uniform manifold and projection (UMAP) (Figure 3A). Based on the expression of *Cd8a*, *Cd8b1*, and *Cd4*, we identified CD8αβ IEL (Cluster 3), CD4^{+} IEL (Clusters 10 and 12), and CD8αα IEL (Clusters 0–2 and 4–8) (Figure 3B). TCRγδ^{+} IEL clustered together with TCRαβ IEL. Among CD8αα IEL, clusters 0 and 5 expressed genes indicative of effector function, such as *Tyrobp*, *Gzma*, and *Gzmb* (Figure 3C). Cluster 1 had a profile similar to those of clusters 0 and 5 but was uniquely enriched for expression of *Gzmk*. Clusters 7 and 8 were characterized by expression of various NK cell receptors such as *Klre1*, *Klra1*, *Klra5, Klra6*, and *Klra7* (Figure 3B, C). Cluster 4 was distinguished by expression of the chemokines *Ccl3* and *Ccl4*. Cluster 9 encompassed proliferating IEL, whereas cluster 13 included *Ifng*-producing IEL. Cluster 2 was marked by expression of the master transcriptional regulators *Tcf7* and *Id3* and was depleted for the effector molecules *Tyrobp* and *Gzma* (Figure 3B, C), a profile similar to that of long-lived memory precursor T cells[40]. Gene Set Enrichment (GSE) analysis corroborated that cluster

2 was enriched for a memory/stem cell signature (Figure S5A). Pseudo time trajectory analysis placed *Tcf7*-expressing IEL at one end of a differentiation hierarchy terminating in several possible effector fates, corroborating a stem-like feature for this population (Figure S5B–D). Further inspection of genes expressed in this cluster revealed that *Ahr* features were abundant in this population relative to other IEL populations, highlighting a potential role for AHR signaling in the function or maintenance of this cell subset (Figure S5E).

Comparison of IEL clusters between WT and *Ahrr*$^{-/-}$ mice revealed a selective expansion of cluster 6 expressing a stress response signature (*Dnajb1, Hspa1a, Hspa1b, Hsph1*) in *Ahrr*$^{-/-}$ mice (Figure 4A–C), whereas the abundance of all other clusters and their transcriptional profiles remained comparable (Figure S5F, G). These results suggested that the number of IEL experiencing oxidative stress was higher in *Ahrr*$^{-/-}$ than WT mice. We confirmed the enhanced expression of the stress response genes *Hspa1a, Hsph1* and *Dnajb1* in CD8αα^{+} IEL by RT-PCR (Figure 4D). One common cause of cell stress is the production of ROS and both HSPA1A and DNAJB1 are considered as markers of oxidative stress[41]. Thus, we examined *Ahrr*$^{-/-}$ IEL for signs of ROS exposure. Indeed, *Ahrr*$^{-/-}$ IEL more highly expressed genes indicating a response to ROS than did WT IEL (Figure 4E). These genes included *Glutathione peroxidase 1* (*Gpx1*), which catalyzes the reduction of lipid peroxides in a glutathione-dependent reaction[42], as well as *Uba52*, which is a ubiquitin gene induced by oxidative stress[43]. Thus, scRNAseq suggested that IEL require AHRR to prevent excessive ROS.

AHRR deficiency causes lipid peroxidation and ferroptosis of IEL

It has been shown that enzymes of the CYP family produce ROS when metabolizing their substrates[31,44]. Moreover, CYPs metabolize arachidonic acid into lipid metabolites that increase NADPH oxidase activity resulting in further ROS production[45–47]. Therefore, we speculated that the oxidative stress response in *Ahrr*$^{-/-}$ IELs may be due to dysregulated induction of the AHR-CYP1A1 axis, leading to increased CYP1A1 enzymatic activity and production of ROS. Supporting this hypothesis, *Cyp1a1* mRNA was more expressed in ileal tissue (Figure 4F) and IEL (Figure 4G) of *Ahrr*$^{-/-}$ mice than in matched tissue and IEL of WT mice. Higher expression was paralleled by increased CYP1A1 enzymatic activity (Figure 4H). We next tested ROS production in IEL. Incubation of different IEL subsets with a substrate indicative of ROS showed that *Ahrr*$^{-/-}$ IEL produced more ROS than did WT IEL (Figure 4I, J). Moreover, treatment with TCDD, a potent AHR ligand and substrate of CYP1A1, induced more cellular ROS in *Ahrr*$^{-/-}$ IEL than in WT IEL (Figure 4K, L). Because ROS has been shown to cause lipid peroxidation and ferroptosis, we further examined whether AHRR deficiency is associated with ferroptosis. To test this, we stained IEL of WT and *Ahrr*$^{-/-}$ mice with C-11 BODIPY, a marker of lipid peroxidation. *Ahrr*$^{-/-}$ IEL evinced a marked increase in lipid peroxidation compared to WT IEL (Figure 4M, N). This finding was further confirmed by both flow cytometry and microscopy using Liperflou, a lipid soluble fluorescent probe that specifically interacts with lipid peroxides and is widely considered a marker of ferroptosis[48] (Figure 4O, P and Figure S6A,B). To directly validate the role of CYP1A1 in inducing ferroptosis, we transduced a T cell line with a CYP1A1-encoding retrovirus and stained cells with C-11 BODIPY. CYP1A1 transduced cells showed increased lipid peroxidation compared to vector transduced cells (Figures S6C). Moreover,

inhibition of CYP1A1 by Rhapontigenin[49] reduced TCDD-induced lipid peroxidation in *Ahrr*$^{-/-}$ IEL (Figure S6D–H). We conclude that *Ahrr* deficiency affects IEL maintenance by causing lipid peroxidation and ferroptosis.

Dietary selenium supplementation rescues IEL loss in *Ahrr*$^{-/-}$ mice

Selenium and selenoproteins have a wide range of cellular functions including the maintenance of redox homeostasis and buffering ROS production, thereby limiting lipid peroxidation and ferroptosis[32]. Thus, we tested whether dietary supplementation of selenium could rescue IEL loss in *Ahrr*$^{-/-}$ mice. WT and *Ahrr*$^{-/-}$ mice were analyzed for lipid peroxidation of IEL by C11-BODIPY staining after adding selenium to the drinking water for 4 weeks (Figure 5A). While mice were on a normal dietary regimen, all subsets of *Ahrr*$^{-/-}$ IEL exhibited higher lipid peroxidation than did WT IEL; however, after selenium supplementation, peroxidation in *Ahrr*$^{-/-}$ IEL was reduced to amounts similar to those of WT IEL (Figure 5B–E). In parallel, selenium supplementation augmented the numbers of all *Ahrr*$^{-/-}$ IEL subsets, including TCR$\alpha\beta^+$ CD8$\alpha\alpha^+$, TCR$\alpha\beta^+$ CD8$\alpha\beta^+$, TCR$\alpha\beta^+$ CD4$^+$ IEL, DP IEL and $\gamma\delta$ T cells, attaining values comparable to those of WT mice (Figure 5F–M). These data corroborate that loss of IEL in *Ahrr*$^{-/-}$ mice is caused by increased ROS generation and consequent ferroptosis.

Inhibition of ROS by dietary Vit-E supplementation restores IEL in *Ahrr*$^{-/-}$ mice

Since Vit-E is a lipid soluble anti-oxidant known to inhibit ferroptosis and lipid peroxidation [32,50], we tested whether Vit-E could rescue IEL loss in *Ahrr*$^{-/-}$ mice. WT and *Ahrr*$^{-/-}$ mice were fed a Vit-E rich diet or normal chow immediately after weaning for 5 weeks (Figure 6A). Lipid peroxidation in IEL was analyzed by C-11 BODIPY staining. *Ahrr*$^{-/-}$ IEL showed more lipid peroxidation than WT IEL subjected when fed normal chow. However, Vit-E supplementation reduced lipid peroxidation of *Ahrr*$^{-/-}$ IEL to the extent of WT IEL (Figure 6B–E). In addition, WT and *Ahrr*$^{-/-}$ mice fed a Vit-E supplemented diet showed comparable IEL abundance, while *Ahrr*$^{-/-}$ mice had lower IEL numbers than WT mice in normal dietary regimen (Figure 6F–M). Collectively, these data demonstrate that *Ahrr* deficiency causes IEL loss by inducing ferroptosis.

Ahrr deficiency increases susceptibility to intestinal pathology

We sought to determine the functional impact of the diminished IEL associated with AHRRdeficiency. Analysis of various inflammatory markers in the ileal tissue in the steady state, such as *Tnfa, Ifng* and *Il6*, divulged similar amounts in *Ahrr*$^{-/-}$ and WT mice, indicating that lack of *Ahrr* does not cause spontaneous tissue inflammation (Figure S7A). We next explored the impact of reduced IEL in *Ahrr*$^{-/-}$ mice in the model of *C. difficile* infection (Figure 7A). Both *Ahrr*$^{-/-}$ and WT mice were treated with antibiotics to induce dysbiosis followed by oral infection with *C. difficile.* Evaluation of clinical score and body weight demonstrated that *Ahrr*$^{-/-}$ mice were more susceptible to *C. difficile* infection than WT mice (Figure 7B, C). Similarly, *Rorc*^{cre} *Ahrr*$^{fl/fl}$ mice, which carry a deletion of *Ahrr* in T cells, were more susceptible to *C. difficile* infection than *Ahrr*$^{fl/fl}$ mice, corroborating that AHRR deficiency has a T cell intrinsic impact (Figure 7D, E). Since IEL promote anti-bacterial responses by releasing inflammatory cytokines and inducing expression of antimicrobial proteins by epithelial cells[3], we measured the mRNA expression of *Ifng*, *Tnfa*,

Il6 and the antimicrobial peptide genes *RegIIIg* and *RegIIIb* in the intestinal tissues upon *C. difficile* infection. *Ahrr*$^{-/-}$ mice expressed much less mRNA from these genes in both colonic and ileal tissues than did WT mice (Figure 7F–I). Because it was previously shown that *Ahrr*$^{-/-}$ mice are more susceptible to DSS-induced colitis[30], we sought to determine whether this was due to a defect of IEL. We compared the severity of DSS-induced colitis in WT mice, *Ahrr*$^{-/-}$ mice and *Ahrr*$^{-/-}$ mice that had been reconstituted with WT IEL 3 days prior to DSS treatment. Analysis of weight loss and colon retraction demonstrated that adoptive transfer of IEL protected *Ahrr*$^{-/-}$ mice from colitis (Figure 7J, K). Altogether, these results demonstrate that IEL reduction in *Ahrr*$^{-/-}$ mice is functionally impactful, increasing their susceptibility to intestinal pathology.

Ahrr is expressed in human intestinal γδ T cells, but less abundantly in IBD

We asked whether AHRR may impact human intestinal T cells. To define organ and cellular distribution of human AHRR, we examined the recently published Cross-Tissue Immune Cell Atlas (CTICA)[51], which contains scRNA-seq data for all known immune cell types in adult humans from a variety of different organs. Across all organs, *Ahrr* was mainly expressed by tissue resident memory γδ T cells and intestinal macrophages (Figure S7B). Because γδ T cells can be found in a variety of different organs, we then plotted the expression of *Ahrr* by all cells grouped by the organ of origin (Figure S7C). Among all organs, caecum, sigmoid colon, ileum, transverse colon, jejunal epithelium and jejunal lamina propria contained cells with the highest expression of *Ahrr*. To further characterize the cells that express *Ahrr* in these organs, we plotted the average expression of *Ahrr* by every cell in each organ (Figure S7D). We found that tissue resident memory γδ T cells expressing abundant *Ahrr* were mainly found in the transverse colon, sigmoid colon, ileum, and caecum. *Ahrr* expression by intestinal γδ T cells was confirmed in a scRNA-seq database generated as part of a human environmental enteropathy study[52] (Figure S7E). To see whether AHRR expression is affected in IBD, we examined a collection of surgical specimens from CD patients that we recently characterized for frequency and function of IEL[53]. Each specimen was divided into macroscopically visibly inflamed and non-inflamed tissue by a pathologist. Less *Ahrr* expression was detected in inflamed tissue from CD patients than in non-inflamed and control tissue (Figure S7F).This observation was consistent with a reduced frequency of γδ T cells we previously reported in the same samples[53]. Thus, AHRR expression inversely correlates with intestinal inflammation, suggesting a possible contribution to pathogenesis that needs to be further explored.

DISCUSSION

The AHR provides a fundamental mechanism by which the epithelium, immune system and nervous system of the intestine sense and respond to various exogenous and endogenous ligands that access the gastrointestinal tract. AHR induces its own negative regulator, AHRR. This study demonstrated that this negative feedback loop was essential for IEL maintenance. AHRR deficiency selectively impaired intestinal IEL in a cell intrinsic fashion, whereas the T cell composition in spleen and MLN was unaffected. scRNA-seq unveiled expansion of cells exposed to oxidative stress among *Ahrr*$^{-/-}$ deficient IEL. AHRR deficiency augmented AHR-mediated induction of CYP1A1 enzymatic activity, resulting

in excessive generation of ROS, which caused lipid peroxidation and ferroptosis in IEL. Conversely, dietary supplementation with anti-oxidative elements - selenium or Vit-E - rescued IEL loss in *Ahrr*$^{-/-}$ mice. Depletion of the IEL compartment in *Ahrr*$^{-/-}$ mice was functionally impactful, heightening susceptibility to intestinal pathology. We conclude that AHR signaling must be tightly regulated to protect IEL from ferroptosis and preserve intestinal immune responses.

Ferroptosis is a type of iron-dependent cell death; it is mainly driven by redox imbalance that leads to excessive iron-dependent lipid peroxidation of membrane phospholipids, especially those with polyunsaturated fatty acids, and ultimately to severe cell membrane dysfunction[54]. While ferroptosis has been extensively demonstrated in tumor cells, there is very limited information regarding its role in T cell biology. One study shows that ferroptosis regulates the homeostasis of follicular helper T (Tfh) cells in the germinal center and that attenuation of ferroptosis by glutathione peroxidase 4 is necessary for Tfh [32]. Our study demonstrates that tight control of lipid peroxidation and ferroptosis by AHRR is necessary to sustain the maintenance of IEL and their capacity to control susceptibility to colitis. This result is consistent with the recent observation that IEL have lower amounts of cellular ROS than memory T cells to be able to be poised to activation while preserving their viability[55].

Our study presents a mechanism by which dysregulated CYP1A1 affects the intestinal immune system, i.e. by inducing excessive ROS production and lipid peroxidation in IEL. Substrate oxidation by NADPH-dependent CYP involves a six-step reaction during which heme-thiolate iron fluctuates between ferric and ferrous forms, interacts with oxygen, and oxidizes the substrate[31,44]. However, the transfer of oxygen to a substrate is not tight, leading to uncoupling and formation of ROS. In addition, CYPs metabolize arachidonic acid to produce 20-hydroxyeicosatetraenoic acid, which increases NADPH oxidase activity resulting in further ROS production[45,46]. In addition to our study, the role of CYPs in production of ROS and cell death has been corroborated in experimental models of heart and liver injury[56–59].

Notably, the dysregulation of AHR-CYP1A1 in *Ahrr*$^{-/-}$ mice selectively affected IEL, while it had no impact on ILC3 or Th17 cells, even though all of these cells express AHRR. Why are IEL so sensitive to AHRR deficiency? The higher expression of *Ahrr* in IEL than lamina propria T cells may in part explain this phenomenon. Moreover, because of their proximity to the intestinal lumen, IELs plausibly have abundant access to AHR ligands to degrade, resulting in substantial production of ROS, whereas ILC3 and Th17 cells may be less exposed to exogenous AHR ligands, resulting in relatively weak activation of the AHR-CYP1A1 axis and modest production of ROS byproducts. The expansion of stressed cells was the fundamental difference between *Ahrr*$^{-/-}$ and WT IEL; no other changes in transcriptional profiles were detected. Hence, our data imply that oxidative stress may be the major cause of IEL reduction and that IEL are particularly sensitive to ROS.

IBD has been associated with alterations in intestinal AHR ligands, such as tryptophan, indole acetic acid (IAA) and kynurenine[60,61], as well as changes in enzymes involved in their generation, such as indoleamine 2,3-dioxygenase (IDO)[62]. The AHR downstream

target CYP1A1 has been found to increase in inflamed tissues of ulcerative colitis and Crohn's disease patients compared to control tissues[63]; moreover, a gain of function mutation in CYP1A1 is associated with UC[64]. Altogether these observations suggest that dysregulated AHR signaling may be deleterious in IBD pathogenesis. Our analysis of human databases and tissues shows that *Ahrr* is highly expressed in human intestinal γδ T cells and that pediatric CD is associated with a concomitant reduction of *Ahrr* expression and γδ T cells. Given the role of AHRR in balancing AHR signaling, reduced expression of AHRR may contribute to IBD pathogenesis by facilitating generation of ROS and ferroptosis in human IEL. Future research will establish whether reduced AHRR expression in IBD is a primary event or secondary to dysregulated AHR signaling associated with IBD pathogenesis.

Limitations of the study

In a previous report, germline deletion of *Ahrr* was associated not only with reduced colonic γδ T cells in the steady state, but also with expansion of intestinal DC during DSS-induced colitis. Alteration of the DC compartment correlated with increased production of IL-1β and expansion of lamina propria Th17 cells, which lowered the Th1/Th17 cell ratio[30]. Furthermore, AHRR deficiency was associated with increased IL-1β production by bone-marrow derived macrophages in vitro. Thus, it will be important to evaluate the impact of AHRR on lamina propria DC and macrophages, particularly their production of inflammatory cytokines and capacity to polarize intestinal T cells in mice with selective deletions of *Ahrr* in DC and macrophages in the context of IBD pathology.

STAR Methods

Resource Availability

Lead contact—Further information and requests for resources and reagents should be directed to and will be fulfilled by Marco Colonna (mcolonna@wustl.edu) upon reasonable request.

Materials availability—This study did not generate any new unique reagents.

Data and code availability—Single-cell RNA-seq data have been deposited at GEO having accession number-GSE199960.

EXPERIMENTAL MODELS

Mice—*Ahrr*$^{fl/fl}$ (*Ahrr*$^{tm1c/tm1c}$) mice and *Ahrr*$^{-/-}$ (*Ahrr*$^{tm1b/tm1b}$) mice were generated in our laboratory from *Ahrr*^{tm1a} sperm (from ES clone *Ahrr* H01) purchased from Eucomm. *Rorc*$^{cre/+}$ mice were kindly provided by Dr. Alexei Tumanov. *Rorc*^{cre}, *Ahrr*$^{fl/fl}$ mice were generated in our animal facility. CD45.1 mice were purchased from Jackson lab. CD45.1/2 mice were generated in our animal facility. WT and *Ahrr*$^{-/-}$ pregnant females were co-housed 1.5–2 weeks before delivery and the pups share the same litter till weaning. After weaning co-housing of WT and *Ahrr*$^{-/-}$ mice were ensured. The animal studies reported in this manuscript were conducted in accordance with guidelines of Washington University animal studies committee. 8–10-week-old mice were used unless otherwise specified.

C. difficile* infection—C. difficile* infection was described in a previous study[65].

METHOD DETAILS

Cell culture—Primary murine cells were cultured in complete RPMI-1640 medium supplemented with 10% BCS, kanamycin, sodium pyruvate, glutamine and nonessential amino acids with and without treatment as mentioned in the figure legends.

Isolation of IEL and lamina propria lymphocytes (LPL)—IEL and LPL were isolated from small intestinal epithelium and lamina propria respectively. Small intestines were flushed with HBSS to remove the fecal content. Peyer's patches were removed followed by longitudinal opening and cut into 1cm pieces. Then, the pieces were washed by gently agitating for 20 minutes followed by vertexing. The flow through was collected and the cycle repeated once again. The flow through was subjected to DTT treatment and Percoll 40–70% gradient separation for isolation of IEL. For LPL isolation, the pieces were rinsed properly with HBSS and then proceeded to digestion with complete RPMI supplemented with collagenase-IV. The undigested tissue chunks were removed by passing through 100-micron mess and then the digests were subjected to 40%–70% Percoll gradient centrifugation for isolation of LPL.

Flow cytometry plots analysis—Cell suspensions were incubated with FC block for 10–15 minutes followed by incubation with cocktail of antibodies for detection of ILC, IEL and T cells. To exclude dead cells the cell suspension was stained with live/dead fixable cell stain kit. For staining of intracellular proteins, cells were fixed and permeabilized using either BD Bioscience fixation/permeabilization Kit (for cytokines) or eBioscience FOXP3 staining kit (for transcription factors) based on the requirement. To identify different IEL populations, IEL were stained with anti-CD45-APC-Cy7, anti-CD3 PACB, anti-CD4-Percp-Cy5.5, anti-CD8α-APC, anti-CD8β-FITC, anti-TCR-γδ-PE. Live, singlet, lymphocyte sized $CD45^{+}$, $CD3^{-}CD5^{-}CD19^{-}$, $ROR\gamma T^{+}$ (ILC3), $GATA3^{high}$ (ILC2) and $ROR\gamma T^{-}$ $GATA3^{int/-}$ as (ILC1 + NK). Identification of different IEL based on different markers described in Figure S1.

Intracellular cytokine analysis—LPL were stimulated with IL-23 for a total of 4 hrs with brefeldin-A for last 3 hours. IEL were stimulated with plastic coated anti-CD3 antibody overnight and incubated with brefeldin-A for the last 3 hours. Then the cells were stained for intracellular cytokines as previously described [37]. Briefly, first the surface staining was performed followed by fixation. Then the cells were permeabilized and stained for intracellular cytokines.

Adoptive transfer of splenic T cells—Splenic T cells from C57BL/6 (CD45.1), WT (CD45.2) and *Ahrr*$^{-/-}$ (CD45.2) mice were isolated using Pan T Cells Isolation Kit (Miltenyi Biotech) according to manufacturer's instruction. Both CD45.1 and CD45.2 cells were mixed together in 1:1 ratio. *Rag1*$^{-/-}$ mice were injected with 10^{6} cells intravenously. Frequencies of CD45.1 vs CD45.2 in different subsets of IEL were analyzed after 8 weeks in the small intestine of recipient mice.

Bone marrow chimera—C57BL/6 (CD45.1/2) mice were lethally irradiated with two cycles of 550 Rads and then were injected with 1×10^6 bone marrow cells from C57BL/6 (CD45.1) along with either WT (CD45.2) or *Ahrr*$^{-/-}$ (CD45.2) in 1:1 ratio. Frequency of different subsets of IEL in the recipient mice were analyzed after 8 weeks.

Q-RT PCR—RNA from Ileal/colonic tissues or sorted cells were isolated using Qiagen RNA easy micro RNA Kit and cDNA synthesized using Quanta bio cDNA synthesis Kit. RT PCR was performed using SYBR green master mix and appropriate primer sets and data were normalized with GAPDH.

ROS detection—2',7'-dichlorodihydrofluorescein diacetate (H2DCFDA) is a chemically reduced form of fluorescein used as an indicator for ROS. Cytosolic ROS was detected by staining the IEL with CM-H2DCFDA (Thermo Fisher) in PBS for 30 min followed by incubation with RPMI media for 1 hr at 37°C. The cells were washed two times with PBS. Surface staining of different IEL markers were performed and analyzed by flow cytometry plots.

C-11 BODIPY and Liperflou staining—IEL from both WT and *Ahrr*$^{-/-}$ mice were surface stained for different markers. Then the cells were incubated with C-11 BODIPY (Thermo Fisher) or Liperflou (Dojindo Labs) for 30 mins at 37°C followed by washing 2 times with PBS and analyzed by flow cytometry plots.

Retroviral transduction—*Cyp1a1* was cloned from the Horizon discovery mammalian gene collection plasmid clone 40129955. The amplicon was then cloned into a MSCV-IRES-Thy1.1 over expression plasmid by Gibson assembly. The control plasmid was empty MSCV-IRES-Thy1.1. Retroviral vectors were transfected into Plat-E cells pseudo typed with the pantropic envelop protein pCL-10A1. Two days after transfection, viral supernatants were collected and separated from cell debris by centrifugation. Jurkat cells were infected with viral supernatants with 2 μg/ml polybrene by 'spin infection' at 700 RCF for 60 min. On day 3, the cells were harvested and analyzed for Thy1.1 expression to evaluate transduction efficiency and further analyzed for lipid peroxidation by C-11 BODIPY staining.

***C. difficile* infection model—**Both WT and *Ahrr*$^{-/-}$ mice were infected with *C. difficile* as previously described [65]. Briefly, mice were administered with antibiotics supplemented drinking water for 4 days followed by clindamycin for 1 day. Then, mice were orally gavaged with *C. difficile* and monitored for clinical manifestations and body weight variation.

DSS induced colitis—Both WT and *Ahrr*$^{-/-}$ mice were administered with 3% DSS (MP Biomedicals) in the drinking water for 7 days. Body weight and colitis associated clinical parameters were monitored every day. 8th day the mice were sacked, and colon length was monitored.

Single cell RNA sequencing—IEL (CD45$^+$, CD3$^+$, CD19$^-$) from two WT and two *Ahrr*$^{-/-}$ 8-week-old male mice were sorted using BD FACS ARIA-II. Sorted cells

were sequenced using the 10x Genomics platform. Cell Ranger pipeline was used to process chromium single-cell RNA-seq output to align reads and generate gene–cell expression matrices (https://support.10xgenomics.com/single-cell-gene-expression/software/overview/welcome). Briefly, short sequencing reads were aligned to the mm10 reference genome and Ensembl transcriptome by STAR. The uniquely aligned reads were used to quantify gene expression for all Ensembl genes. We filtered out low-quality cells from the dataset if the number of UMI was fewer than 1000 or genes detected was fewer than 500. Cells with low complexity (< 0.8), as defined by the fraction of genes over UMI, were filtered out. We also excluded those cells with a high percentage of mitochondrion reads (>20%). In addition, all genes that were not detected in at least 10 of all the single cells were discarded. After quality control, data from two mice in each group were pooled together; total 10,613 WT and 14,882 *Ahr*$^{-/-}$ IEL were subjected to final analysis. Data analyses were performed using the R software package Seurat (http://satijalab.org/seurat/) [66]. Data were scaled and transformed and variable genes identified using the SC Transform function [67], and linear regression was performed to remove unwanted variation due to cell quality (% mitochondrial reads. Data from both genotypes were then integrated using the top 3000 variable features and principal component analysis was performed using these variable genes, and the first 40 principal components (PCs) were used to perform UMAP to embed the dataset into two dimensions. Next, the first 40 PCs were used to construct a shared nearest-neighbor graph (SNN; Find Neighbors) and this SNN was used to cluster the dataset (Find Clusters (resolution = 0.4)) using a graph-based modularity-optimization algorithm of the Louvain method for community detection. Despite sorting on CD3^{+} cells, minor clusters of contaminating B cells and myeloid cells were identified and removed for downstream analysis. After filtering out contaminating cell types, PCA, UMAP, and clustering analysis were redone using the same parameters as above. Cellular identity was determined by finding DE genes for each cluster using Seurat's implementation of the Wilcoxon rank-sum test (Find Markers) and comparing those markers to known cell type-specific genes from previous datasets. Differential gene analysis comparing IEL from different genotypes was performed using the R package MAST[68].

Statistical analysis—Two experimental groups were compared by Mann-Whitney U test. Statistical analysis was performed using GraphPad prism software (version 7). P<0.05 was considered statistically significant. * P<0.05, ** P<0.01, *** p< 0.001.

Supplementary Material

Refer to Web version on PubMed Central for supplementary material.

ACKNOWLEDGEMENTS

The work was supported by NIH (R01 DE025884, R01 AI134236, and R01 AI134035) to Marco Colonna. The authors would like to thank Jennifer K. Bando and Wei-Le Wang for helpful discussions.

REFERENCES

1. Cheroutre H, Lambolez F, and Mucida D (2011). The light and dark sides of intestinal intraepithelial lymphocytes. Nat Rev Immunol 11, 445–456. nri3007 [pii]10.1038/nri3007. [PubMed: 21681197]

2. Li Y, Innocentin S, Withers DR, Roberts NA, Gallagher AR, Grigorieva EF, Wilhelm C, and Veldhoen M (2011). Exogenous stimuli maintain intraepithelial lymphocytes via aryl hydrocarbon receptor activation. Cell 147, 629–640. S0092–8674(11)01136–6 [pii]10.1016/j.cell.2011.09.025. [PubMed: 21999944]
3. Shui JW, Larange A, Kim G, Vela JL, Zahner S, Cheroutre H, and Kronenberg M (2012). HVEM signalling at mucosal barriers provides host defence against pathogenic bacteria. Nature 488, 222–225. nature11242 [pii]10.1038/nature11242. [PubMed: 22801499]
4. Pope C, Kim SK, Marzo A, Masopust D, Williams K, Jiang J, Shen H, and Lefrancois L (2001). Organ-specific regulation of the CD8 T cell response to Listeria monocytogenes infection. J Immunol 166, 3402–3409. 10.4049/jimmunol.166.5.3402. [PubMed: 11207297]
5. Van Kaer L, Algood HMS, Singh K, Parekh VV, Greer MJ, Piazuelo MB, Weitkamp JH, Matta P, Chaturvedi R, Wilson KT, and Olivares-Villagomez D (2014). CD8alphaalpha(+) innate-type lymphocytes in the intestinal epithelium mediate mucosal immunity. Immunity 41, 451–464. S1074–7613(14)00304–5 [pii]10.1016/j.immuni.2014.08.010. [PubMed: 25220211]
6. Sujino T, London M, Hoytema van Konijnenburg DP, Rendon T, Buch T, Silva HM, Lafaille JJ, Reis BS, and Mucida D (2016). Tissue adaptation of regulatory and intraepithelial CD4(+) T cells controls gut inflammation. Science 352, 1581–1586. science.aaf3892 [pii]10.1126/science.aaf3892. [PubMed: 27256884]
7. Klose CS, Blatz K, d'Hargues Y, Hernandez PP, Kofoed-Nielsen M, Ripka JF, Ebert K, Arnold SJ, Diefenbach A, Palmer E, and Tanriver Y (2014). The transcription factor T-bet is induced by IL-15 and thymic agonist selection and controls CD8alphaalpha(+) intraepithelial lymphocyte development. Immunity 41, 230–243. S1074–7613(14)00274-X [pii]10.1016/j.immuni.2014.06.018. [PubMed: 25148024]
8. Das G, Augustine MM, Das J, Bottomly K, Ray P, and Ray A (2003). An important regulatory role for CD4+CD8 alpha alpha T cells in the intestinal epithelial layer in the prevention of inflammatory bowel disease. Proc Natl Acad Sci U S A 100, 5324–5329. 10.1073/pnas.0831037100 0831037100 [pii]. [PubMed: 12695566]
9. Liu L, Gong T, Tao W, Lin B, Li C, Zheng X, Zhu S, Jiang W, and Zhou R (2019). Commensal viruses maintain intestinal intraepithelial lymphocytes via noncanonical RIG-I signaling. Nat Immunol 20, 1681–1691. 10.1038/s41590-019-0513-z10.1038/s41590-019-0513-z [pii]. [PubMed: 31636462]
10. Cervantes-Barragan L, and Colonna M (2018). AHR signaling in the development and function of intestinal immune cells and beyond. Semin Immunopathol 40, 371–377. 10.1007/s00281-018-0694-910.1007/s00281-018-0694-9 [pii]. [PubMed: 29951906]
11. Rothhammer V, and Quintana FJ (2019). The aryl hydrocarbon receptor: an environmental sensor integrating immune responses in health and disease. Nat Rev Immunol 19, 184–197. 10.1038/s41577-019-0125-810.1038/s41577-019-0125-8 [pii]. [PubMed: 30718831]
12. DiNatale BC, Murray IA, Schroeder JC, Flaveny CA, Lahoti TS, Laurenzana EM, Omiecinski CJ, and Perdew GH (2010). Kynurenic acid is a potent endogenous aryl hydrocarbon receptor ligand that synergistically induces interleukin-6 in the presence of inflammatory signaling. Toxicol Sci 115, 89–97. 10.1093/toxsci/kfq024. [PubMed: 20106948]
13. Stockinger B, Di Meglio P, Gialitakis M, and Duarte JH (2014). The aryl hydrocarbon receptor: multitasking in the immune system. Annu Rev Immunol 32, 403–432. 10.1146/annurev-immunol-032713-120245. [PubMed: 24655296]
14. Beedanagari SR, Bebenek I, Bui P, and Hankinson O (2009). Resveratrol inhibits dioxin-induced expression of human CYP1A1 and CYP1B1 by inhibiting recruitment of the aryl hydrocarbon receptor complex and RNA polymerase II to the regulatory regions of the corresponding genes. Toxicol Sci 110, 61–67. 10.1093/toxsci/kfp079. [PubMed: 19376845]
15. Mescher M, and Haarmann-Stemmann T (2018). Modulation of CYP1A1 metabolism: From adverse health effects to chemoprevention and therapeutic options. Pharmacol Ther 187, 71–87. 10.1016/j.pharmthera.2018.02.012. [PubMed: 29458109]
16. Lucas D, Goulitquer S, Marienhagen J, Fer M, Dreano Y, Schwaneberg U, Amet Y, and Corcos L (2010). Stereoselective epoxidation of the last double bond of polyunsaturated fatty acids by human cytochromes P450. J Lipid Res 51, 1125–1133. 10.1194/jlr.M003061. [PubMed: 19965576]

17. Cervantes-Barragan L, Chai JN, Tianero MD, Di Luccia B, Ahern PP, Merriman J, Cortez VS, Caparon MG, Donia MS, Gilfillan S, et al. (2017). Lactobacillus reuteri induces gut intraepithelial CD4(+)CD8alphaalpha(+) T cells. Science 357, 806–810. science.aah5825 [pii]10.1126/science.aah5825. [PubMed: 28775213]

18. Metidji A, Omenetti S, Crotta S, Li Y, Nye E, Ross E, Li V, Maradana MR, Schiering C, and Stockinger B (2018). The Environmental Sensor AHR Protects from Inflammatory Damage by Maintaining Intestinal Stem Cell Homeostasis and Barrier Integrity. Immunity 49, 353–362 e355. S1074–7613(18)30330–3 [pii]10.1016/j.immuni.2018.07.010. [PubMed: 30119997]

19. Kimura A, Naka T, Nohara K, Fujii-Kuriyama Y, and Kishimoto T (2008). Aryl hydrocarbon receptor regulates Stat1 activation and participates in the development of Th17 cells. Proc Natl Acad Sci U S A 105, 9721–9726. 0804231105 [pii] 10.1073/pnas.0804231105. [PubMed: 18607004]

20. Quintana FJ, Basso AS, Iglesias AH, Korn T, Farez MF, Bettelli E, Caccamo M, Oukka M, and Weiner HL (2008). Control of T(reg) and T(H)17 cell differentiation by the aryl hydrocarbon receptor. Nature 453, 65–71. nature06880 [pii]10.1038/nature06880. [PubMed: 18362915]

21. Apetoh L, Quintana FJ, Pot C, Joller N, Xiao S, Kumar D, Burns EJ, Sherr DH, Weiner HL, and Kuchroo VK (2010). The aryl hydrocarbon receptor interacts with c-Maf to promote the differentiation of type 1 regulatory T cells induced by IL-27. Nat Immunol 11, 854–861. ni.1912 [pii]10.1038/ni.1912. [PubMed: 20676095]

22. Qiu J, Heller JJ, Guo X, Chen ZM, Fish K, Fu YX, and Zhou L (2012). The aryl hydrocarbon receptor regulates gut immunity through modulation of innate lymphoid cells. Immunity 36, 92–104. S1074–7613(11)00505-X [pii]10.1016/j.immuni.2011.11.011. [PubMed: 22177117]

23. Kiss EA, Vonarbourg C, Kopfmann S, Hobeika E, Finke D, Esser C, and Diefenbach A (2011). Natural aryl hydrocarbon receptor ligands control organogenesis of intestinal lymphoid follicles. Science 334, 1561–1565. 10.1126/science.1214914. [PubMed: 22033518]

24. Lee JS, Cella M, McDonald KG, Garlanda C, Kennedy GD, Nukaya M, Mantovani A, Kopan R, Bradfield CA, Newberry RD, and Colonna M (2011). AHR drives the development of gut ILC22 cells and postnatal lymphoid tissues via pathways dependent on and independent of Notch. Nat Immunol 13, 144–151. ni.2187 [pii]10.1038/ni.2187. [PubMed: 22101730]

25. Li S, Bostick JW, Ye J, Qiu J, Zhang B, Urban JF Jr., Avram D, and Zhou L (2018). Aryl Hydrocarbon Receptor Signaling Cell Intrinsically Inhibits Intestinal Group 2 Innate Lymphoid Cell Function. Immunity 49, 915–928 e915. S1074–7613(18)30430–8 [pii]10.1016/j.immuni.2018.09.015. [PubMed: 30446384]

26. Obata Y, Castano A, Boeing S, Bon-Frauches AC, Fung C, Fallesen T, de Aguero MG, Yilmaz B, Lopes R, Huseynova A, et al. (2020). Neuronal programming by microbiota regulates intestinal physiology. Nature 578, 284–289. 10.1038/s41586-020-1975-810.1038/s41586-020-1975-8 [pii]. [PubMed: 32025031]

27. Schiering C, Wincent E, Metidji A, Iseppon A, Li Y, Potocnik AJ, Omenetti S, Henderson CJ, Wolf CR, Nebert DW, and Stockinger B (2017). Feedback control of AHR signalling regulates intestinal immunity. Nature 542, 242–245. nature21080 [pii]10.1038/nature21080. [PubMed: 28146477]

28. Haarmann-Stemmann T, Bothe H, Kohli A, Sydlik U, Abel J, and Fritsche E (2007). Analysis of the transcriptional regulation and molecular function of the aryl hydrocarbon receptor repressor in human cell lines. Drug Metab Dispos 35, 2262–2269. dmd.107.016253 [pii]10.1124/dmd.107.016253. [PubMed: 17890447]

29. Baba T, Mimura J, Gradin K, Kuroiwa A, Watanabe T, Matsuda Y, Inazawa J, Sogawa K, and Fujii-Kuriyama Y (2001). Structure and expression of the Ah receptor repressor gene. J Biol Chem 276, 33101–33110. 10.1074/jbc.M011497200M011497200 [pii]. [PubMed: 11423533]

30. Brandstatter O, Schanz O, Vorac J, Konig J, Mori T, Maruyama T, Korkowski M, Haarmann-Stemmann T, von Smolinski D, Schultze JL, et al. (2016). Balancing intestinal and systemic inflammation through cell type-specific expression of the aryl hydrocarbon receptor repressor. Sci Rep 6, 26091. srep26091 [pii]10.1038/srep26091. [PubMed: 27184933]

31. Veith A, and Moorthy B (2018). Role of Cytochrome P450s in the Generation and Metabolism of Reactive Oxygen Species. Curr Opin Toxicol 7, 44–51. 10.1016/j.cotox.2017.10.003. [PubMed: 29527583]

32. Yao Y, Chen Z, Zhang H, Chen C, Zeng M, Yunis J, Wei Y, Wan Y, Wang N, Zhou M, et al. (2021). Selenium-GPX4 axis protects follicular helper T cells from ferroptosis. Nat Immunol 22, 1127–1139. 10.1038/s41590-021-00996-0. [PubMed: 34413521]
33. Reis BS, Rogoz A, Costa-Pinto FA, Taniuchi I, and Mucida D (2013). Mutual expression of the transcription factors Runx3 and ThPOK regulates intestinal CD4(+) T cell immunity. Nat Immunol 14, 271–280. ni.2518 [pii]10.1038/ni.2518. [PubMed: 23334789]
34. Mayassi T, and Jabri B (2018). Human intraepithelial lymphocytes. Mucosal Immunol 11, 1281–1289. 10.1038/s41385-018-0016-5. [PubMed: 29674648]
35. Lahvis GP, Pyzalski RW, Glover E, Pitot HC, McElwee MK, and Bradfield CA (2005). The aryl hydrocarbon receptor is required for developmental closure of the ductus venosus in the neonatal mouse. Mol Pharmacol 67, 714–720. mol.104.008888 [pii]10.1124/mol.104.008888. [PubMed: 15590894]
36. Andersson P, McGuire J, Rubio C, Gradin K, Whitelaw ML, Pettersson S, Hanberg A, and Poellinger L (2002). A constitutively active dioxin/aryl hydrocarbon receptor induces stomach tumors. Proc Natl Acad Sci U S A 99, 9990–9995. 10.1073/pnas.152706299152706299 [pii]. [PubMed: 12107286]
37. Cortez VS, Cervantes-Barragan L, Song C, Gilfillan S, McDonald KG, Tussiwand R, Edelson BT, Murakami Y, Murphy KM, Newberry RD, et al. (2014). CRTAM controls residency of gut CD4+CD8+ T cells in the steady state and maintenance of gut CD4+ Th17 during parasitic infection. J Exp Med 211, 623–633. jem.20130904 [pii]10.1084/jem.20130904. [PubMed: 24687959]
38. Gangadharan D, Lambolez F, Attinger A, Wang-Zhu Y, Sullivan BA, and Cheroutre H (2006). Identification of pre- and postselection TCRalphabeta+ intraepithelial lymphocyte precursors in the thymus. Immunity 25, 631–641. S1074–7613(06)00429–8 [pii]10.1016/j.immuni.2006.08.018. [PubMed: 17045820]
39. Golec DP, Hoeppli RE, Henao Caviedes LM, McCann J, Levings MK, and Baldwin TA (2017). Thymic progenitors of TCRalphabeta(+) CD8alphaalpha intestinal intraepithelial lymphocytes require RasGRP1 for development. J Exp Med 214, 2421–2435. jem.20170844 [pii]10.1084/jem.20170844. [PubMed: 28652304]
40. Zhou X, Yu S, Zhao DM, Harty JT, Badovinac VP, and Xue HH (2010). Differentiation and persistence of memory CD8(+) T cells depend on T cell factor 1. Immunity 33, 229–240. S1074–7613(10)00285–2 [pii]10.1016/j.immuni.2010.08.002. [PubMed: 20727791]
41. Barrett MJ, Alones V, Wang KX, Phan L, and Swerdlow RH (2004). Mitochondria-derived oxidative stress induces a heat shock protein response. J Neurosci Res 78, 420–429. 10.1002/jnr.20249. [PubMed: 15389841]
42. Lei XG, Cheng WH, and McClung JP (2007). Metabolic regulation and function of glutathione peroxidase-1. Annu Rev Nutr 27, 41–61. 10.1146/annurev.nutr.27.061406.093716. [PubMed: 17465855]
43. Fernandes R, Ramalho J, and Pereira P (2006). Oxidative stress upregulates ubiquitin proteasome pathway in retinal endothelial cells. Mol Vis 12, 1526–1535. [PubMed: 17167411]
44. Hrycay EG, and Bandiera SM (2015). Monooxygenase, peroxidase and peroxygenase properties and reaction mechanisms of cytochrome P450 enzymes. Adv Exp Med Biol 851, 1–61. 10.1007/978-3-319-16009-2_1. [PubMed: 26002730]
45. Zeng Q, Han Y, Bao Y, Li W, Li X, Shen X, Wang X, Yao F, O'Rourke ST, and Sun C (2010). 20-HETE increases NADPH oxidase-derived ROS production and stimulates the L-type Ca2+ channel via a PKC-dependent mechanism in cardiomyocytes. Am J Physiol Heart Circ Physiol 299, H1109–1117. 10.1152/ajpheart.00067.2010. [PubMed: 20675568]
46. Han Y, Zhao H, Tang H, Li X, Tan J, Zeng Q, and Sun C (2013). 20-Hydroxyeicosatetraenoic acid mediates isolated heart ischemia/reperfusion injury by increasing NADPH oxidase-derived reactive oxygen species production. Circ J 77, 1807–1816. 10.1253/circj.cj-12-1211. [PubMed: 23585488]
47. Zou Y, Li H, Graham ET, Deik AA, Eaton JK, Wang W, Sandoval-Gomez G, Clish CB, Doench JG, and Schreiber SL (2020). Cytochrome P450 oxidoreductase contributes to phospholipid peroxidation in ferroptosis. Nat Chem Biol 16, 302–309. 10.1038/s41589-020-0472-6. [PubMed: 32080622]

48. Kagan VE, Mao G, Qu F, Angeli JP, Doll S, Croix CS, Dar HH, Liu B, Tyurin VA, Ritov VB, et al. (2017). Oxidized arachidonic and adrenic PEs navigate cells to ferroptosis. Nat Chem Biol 13, 81–90. 10.1038/nchembio.2238. [PubMed: 27842066]
49. Chun YJ, Ryu SY, Jeong TC, and Kim MY (2001). Mechanism-based inhibition of human cytochrome P450 1A1 by rhapontigenin. Drug Metab Dispos 29, 389–393. [PubMed: 11259321]
50. Matsushita M, Freigang S, Schneider C, Conrad M, Bornkamm GW, and Kopf M (2015). T cell lipid peroxidation induces ferroptosis and prevents immunity to infection. J Exp Med 212, 555–568. 10.1084/jem.20140857. [PubMed: 25824823]
51. Dominguez Conde C, Xu C, Jarvis LB, Rainbow DB, Wells SB, Gomes T, Howlett SK, Suchanek O, Polanski K, King HW, et al. (2022). Cross-tissue immune cell analysis reveals tissue-specific features in humans. Science 376, eabl5197. 10.1126/science.abl5197. [PubMed: 35549406]
52. Kummerlowe C, Wallach T, Mwakamui S, Hughes TK, Mulugeta N, Mudenda V, Besa E, Zyambo K, Fleming I, Vukovic M, et al. (2021). Single-cell profiling of environmental enteropathy reveals signatures of epithelial remodeling and immune activation in severe disease. bioRxiv, 2021.2004.2011.439202. 10.1101/2021.04.11.439202.
53. Jaeger N, Gamini R, Cella M, Schettini JL, Bugatti M, Zhao S, Rosadini CV, Esaulova E, Di Luccia B, Kinnett B, et al. (2021). Single-cell analyses of Crohn's disease tissues reveal intestinal intraepithelial T cells heterogeneity and altered subset distributions. Nat Commun 12, 1921. 10.1038/s41467-021-22164-6. [PubMed: 33771991]
54. Stockwell BR, Friedmann Angeli JP, Bayir H, Bush AI, Conrad M, Dixon SJ, Fulda S, Gascon S, Hatzios SK, Kagan VE, et al. (2017). Ferroptosis: A Regulated Cell Death Nexus Linking Metabolism, Redox Biology, and Disease. Cell 171, 273–285. 10.1016/j.cell.2017.09.021. [PubMed: 28985560]
55. Konjar S, Frising UC, Ferreira C, Hinterleitner R, Mayassi T, Zhang Q, Blankenhaus B, Haberman N, Loo Y, Guedes J, et al. (2018). Mitochondria maintain controlled activation state of epithelial-resident T lymphocytes. Sci Immunol 3. 10.1126/sciimmunol.aan2543.
56. Granville DJ, Tashakkor B, Takeuchi C, Gustafsson AB, Huang C, Sayen MR, Wentworth P Jr., Yeager M, and Gottlieb RA (2004). Reduction of ischemia and reperfusion-induced myocardial damage by cytochrome P450 inhibitors. Proc Natl Acad Sci U S A 101, 1321–1326. 10.1073/pnas.0308185100. [PubMed: 14734800]
57. Shaik IH, and Mehvar R (2010). Effects of cytochrome p450 inhibition by cimetidine on the warm hepatic ischemia-reperfusion injury in rats. J Surg Res 159, 680–688. 10.1016/j.jss.2008.09.016. [PubMed: 19500799]
58. Shaik IH, and Mehvar R (2010). Cytochrome P450 induction by phenobarbital exacerbates warm hepatic ischemia-reperfusion injury in rat livers. Free Radic Res 44, 441–453. 10.3109/10715761003610729. [PubMed: 20166883]
59. Ishihara Y, Sekine M, Hamaguchi A, Kobayashi Y, Harayama T, Nakazawa M, and Shimamoto N (2010). Effects of sulfaphenazole derivatives on cardiac ischemia-reperfusion injury: association of cytochrome P450 activity and infarct size. J Pharmacol Sci 113, 335–342. 10.1254/jphs.10103fp. [PubMed: 20644334]
60. Lamas B, Richard ML, Leducq V, Pham HP, Michel ML, Da Costa G, Bridonneau C, Jegou S, Hoffmann TW, Natividad JM, et al. (2016). CARD9 impacts colitis by altering gut microbiota metabolism of tryptophan into aryl hydrocarbon receptor ligands. Nat Med 22, 598–605. 10.1038/nm.4102. [PubMed: 27158904]
61. Nikolaus S, Schulte B, Al-Massad N, Thieme F, Schulte DM, Bethge J, Rehman A, Tran F, Aden K, Hasler R, et al. (2017). Increased Tryptophan Metabolism Is Associated With Activity of Inflammatory Bowel Diseases. Gastroenterology 153, 1504–1516 e1502. 10.1053/j.gastro.2017.08.028. [PubMed: 28827067]
62. Sofia MA, Ciorba MA, Meckel K, Lim CK, Guillemin GJ, Weber CR, Bissonnette M, and Pekow JR (2018). Tryptophan Metabolism through the Kynurenine Pathway is Associated with Endoscopic Inflammation in Ulcerative Colitis. Inflamm Bowel Dis 24, 1471–1480. 10.1093/ibd/izy103. [PubMed: 29796641]
63. Sen A, and Stark H (2019). Role of cytochrome P450 polymorphisms and functions in development of ulcerative colitis. World J Gastroenterol 25, 2846–2862. 10.3748/wjg.v25.i23.2846. [PubMed: 31249444]

64. Buyukgoze O, Osmanoglu N, Arslan S, and Sen A (2013). Association of the CYP1A1*2A, GSTT1 null, GSTM1 null, mEPHX*3, and XRCC1–399 genetic polymorphisms with ulcerative colitis. Int J Colorectal Dis 28, 593–595. 10.1007/s00384-012-1507-6. [PubMed: 22664944]

65. Fachi JL, Secca C, Rodrigues PB, Mato FCP, Di Luccia B, Felipe JS, Pral LP, Rungue M, Rocha VM, Sato FT, et al. (2020). Acetate coordinates neutrophil and ILC3 responses against C. difficile through FFAR2. J Exp Med 217. 133544 [pii]10.1084/jem.20190489.

66. Butler A, Hoffman P, Smibert P, Papalexi E, and Satija R (2018). Integrating single-cell transcriptomic data across different conditions, technologies, and species. Nat Biotechnol 36, 411–420. nbt.4096 [pii]10.1038/nbt.4096. [PubMed: 29608179]

67. Hafemeister C, and Satija R (2019). Normalization and variance stabilization of single-cell RNA-seq data using regularized negative binomial regression. Genome Biol 20, 296. 10.1186/s13059-019-1874-110.1186/s13059-019-1874-1 [pii]. [PubMed: 31870423]

68. Finak G, McDavid A, Yajima M, Deng J, Gersuk V, Shalek AK, Slichter CK, Miller HW, McElrath MJ, Prlic M, et al. (2015). MAST: a flexible statistical framework for assessing transcriptional changes and characterizing heterogeneity in single-cell RNA sequencing data. Genome Biol 16, 278. 10.1186/s13059-015-0844-510.1186/s13059-015-0844-5 [pii]. [PubMed: 26653891]

Highlights

- Intestinal IELs decline in the absence of *Ahrr* in a cell-intrinsic fashion.
- Lack of *Ahrr* fuels CYP1A1 oxygenase activity, lipid peroxidation, and ferroptosis.
- Restoration of redox homeostasis by dietary anti-oxidants rescues IEL numbers.
- Fewer IELs, due to an *Ahrr* defect, provoke intestinal infection and inflammation.

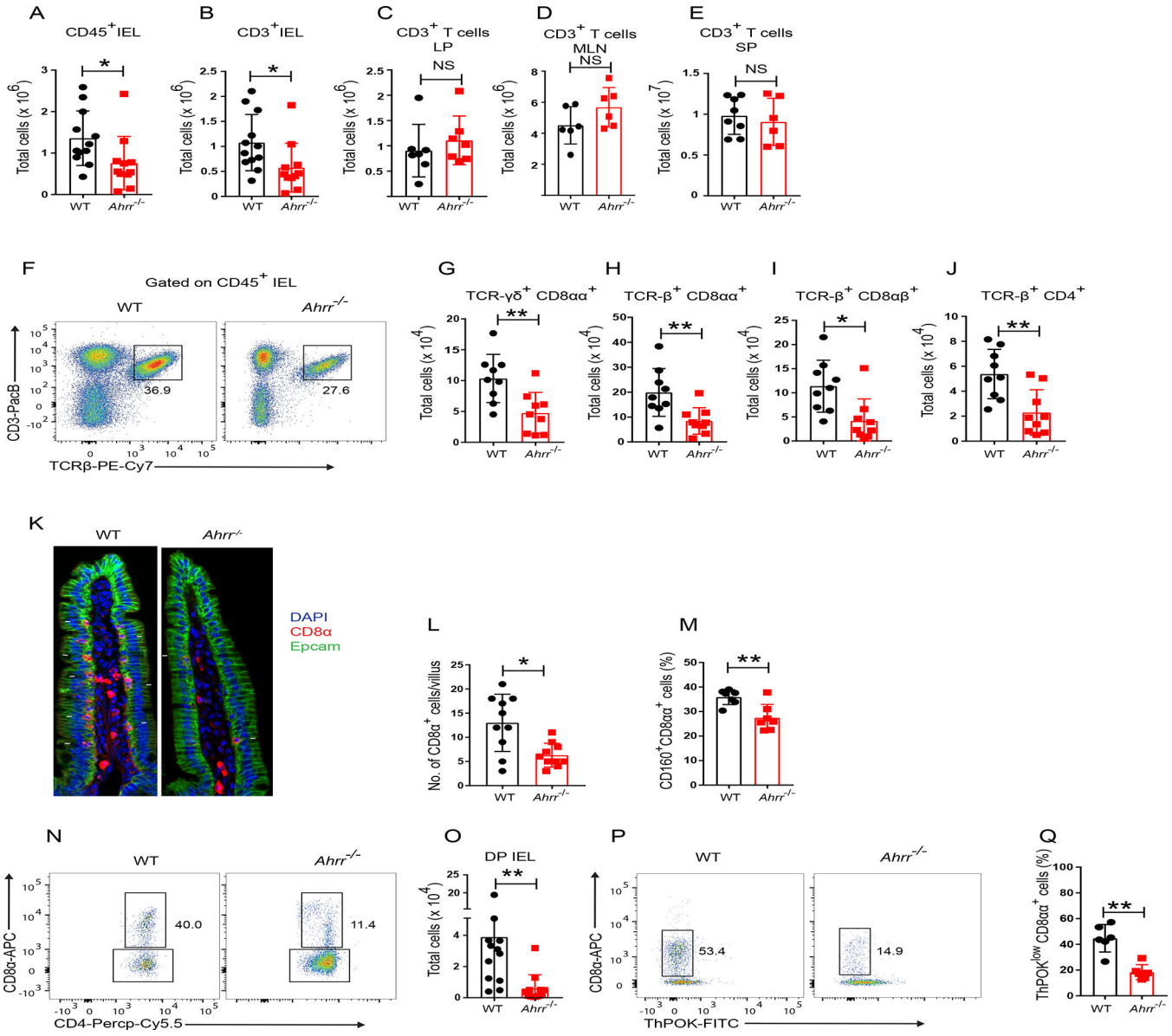

Figure 1. *Ahrr*$^{-/-}$ mice have reduced numbers of IEL.

(A) Numbers of CD45^{+} IEL in the small intestine of WT and *Ahrr*$^{-/-}$ mice. **(B-E)** Numbers of T cells in small intestinal epithelium **(B)**, small intestinal lamina propria **(C)**, mesenteric lymph nodes **(D)** and spleen **(E)** of WT and *Ahrr*$^{-/-}$ mice. **(F)** Representative flow cytometry plots depicting frequency of TCR-β^{+} IEL in WT and *Ahrr*$^{-/-}$ mice. **(G-J)** IEL populations in small intestinal epithelium of WT and *Ahrr*$^{-/-}$ mice, including TCR-γδ^{+} CD8αα^{+} **(G)**, TCR-β^{+} CD8αα^{+} **(H)**, TCR-β^{+} CD8αβ^{+} **(I)**, and TCR-β^{+} CD4^{+} **(J)**. **(K)** Immunofluorescence staining of CD8α in the small intestine of WT and *Ahrr*$^{-/-}$ mice. **(l)** Quantification of CD8α+ cells per villus of WT and *Ahrr*$^{-/-}$ mice. **(M)** Frequency of CD160^{+} TCR-β^{+} CD8αα^{+} IELs in WT and *Ahrr*$^{-/-}$ mice. **(N, O)** Representative flow cytometry plots **(N)** and numbers of DP IEL **(O)** in WT and *Ahrr*$^{-/-}$ mice (gated on CD45^{+}, CD3^{+}, TCR γδ^{-}, TCRαβ^{+}, CD8β^{-} CD4^{+} IEL). **(P and Q)** Representative flow

cytometry plots plots **(P)** and frequency of ThPOK^{low} CD8αα^{+} cells **(Q)** in WT and *Ahrr*$^{-/-}$ mice. Each dot represents an individual mouse. Data are pool or representative of 2–3 individual experiments. Statistical significance was determined by Mann-Whitney test. *P<0.05, **P<0.01. Please also see Figures S1 and S2.

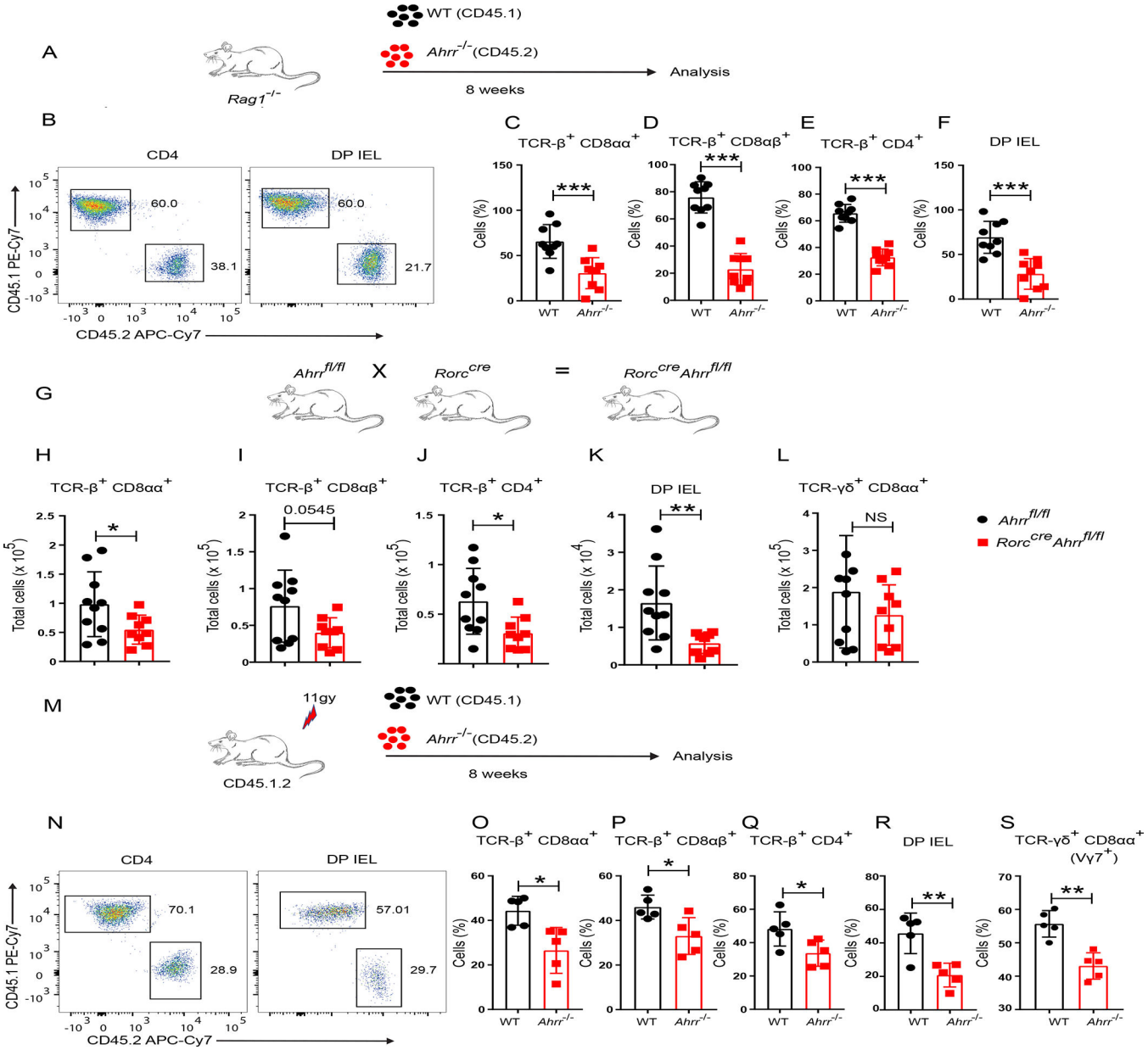

Figure 2. Loss of IEL in *Ahrr*$^{-/-}$ mice is cell intrinsic.

(A) Schematic of the experiment. Purified splenic T cells from WT (CD45.1) and *Ahrr*$^{-/-}$ (CD45.2) were transferred to *Rag1*$^{-/-}$ mice in 1:1 ratio and IEL were analyzed after 8 weeks. **(B)** Representative flow cytometry plots plots showing CD4^{+} T cells and DP IEL from small intestine of reconstituted mice. **(C-F)** Frequency of WT and *Ahrr*$^{-/-}$ TCR-β^{+} CD8αα^{+} **(C)**, TCR-β^{+} CD8αβ^{+} **(D)**, TCR-β^{+} CD4^{+} **(E)**, and DP IEL **(F)**, in the small intestine IEL of *Rag1*$^{-/-}$ mice after reconstitution. **(G)** *Rorc*^{cre} *Ahrr*$^{fl/fl}$ mice were generated by mating *Rorc*^{cre} with *Ahrr*$^{fl/fl}$ mice. **(H-L)** Cell numbers of TCR-β^{+} CD8αα^{+} **(H)**, TCR-β^{+} CD8αβ^{+} **(I)**, TCR-β^{+} CD4^{+} **(J)**, DP IEL **(K)**, and TCR-γδ^{+} CD8αα^{+} **(L)**, in *Ahrr*$^{fl/fl}$ and *Rorc*^{cre} *Ahrr*$^{fl/fl}$ mice. **(M)** Schematic of the experiment: IEL from the small intestine of chimeric mice reconstituted with bone marrow cells from WT (CD45.1) and

Ahrr$^{-/-}$ (CD45.2) mice in 1:1 ratio. **(N)** Representative flow cytometry plots showing CD4^{+} T cells and DP IEL from small intestine of reconstituted mice. **o-s**, Frequencies of WT and *Ahrr*$^{-/-}$ TCR-β^{+} CD8αα^{+} **(O)**; TCR-β^{+} CD8 αβ^{+} **(P)**, TCR-β^{+} CD4^{+} **(Q)**, DP IEL **(R)**, and γδ (vγ7^{+}) IEL **(S)**, in small intestinal epithelium of bone marrow chimeric mice. Each dot represents an individual mouse. Data are pool or representative of 2 individual experiments. Statistical significance was determined by Mann-Whitney test. *P<0.05, **P<0.01, ***P<0.001. Please also see Figure S3.

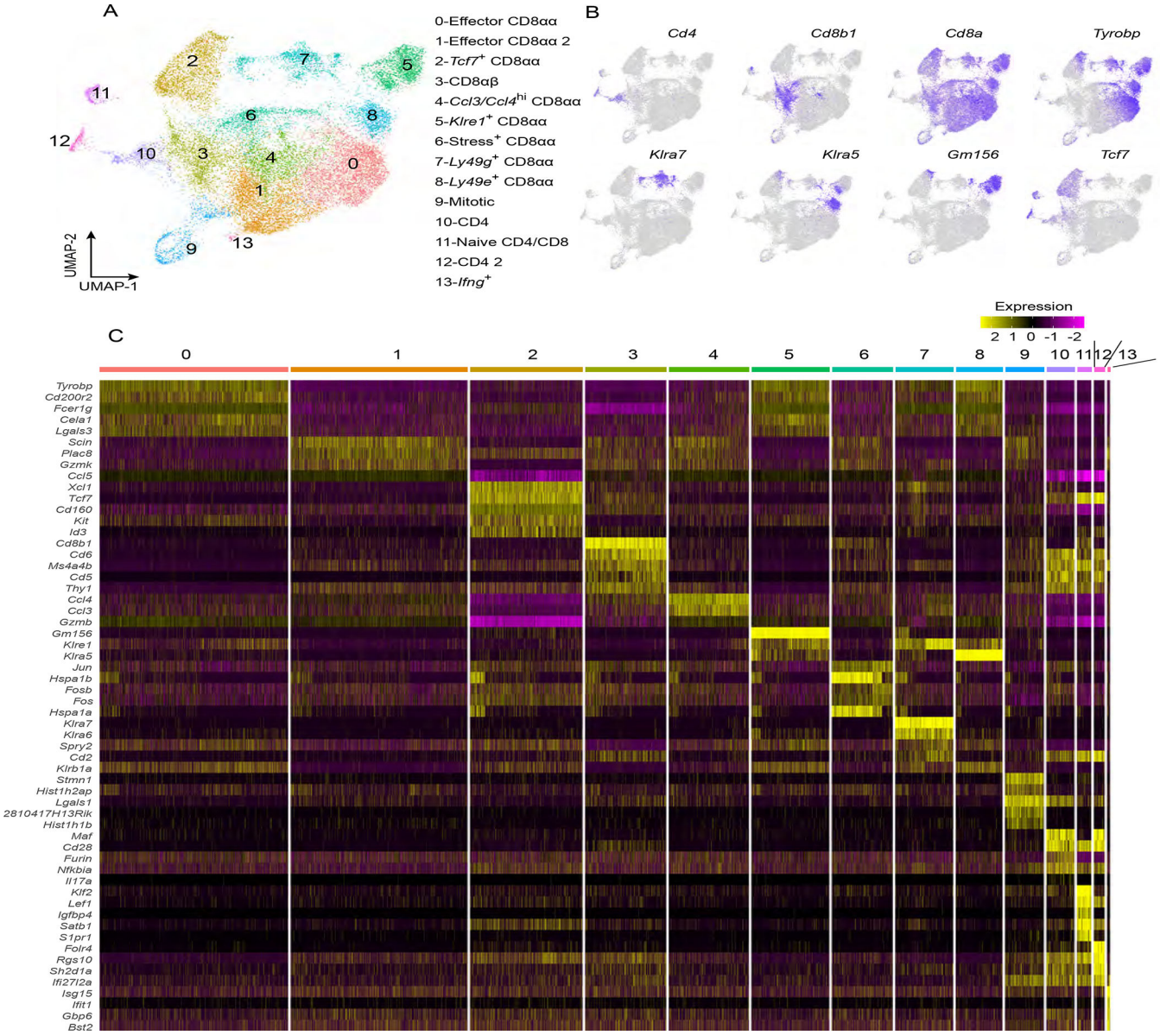

Figure 3. scRNAseq of WT and *Ahrr*$^{-/-}$ IEL.

IEL (CD45^{+} CD3^{+} CD19^{-}) from both WT and *Ahrr*$^{-/-}$ mice were subjected to single cell RNA sequencing analysis. **(A)** UMAP plot depicting various populations of IEL. **(B)** Feature plots depicting expression of *Cd4*, *Cd8b*, *Cd8a, Tyrobp, Klra7, Klra5, Gm156* and *Tcf7.* **(C)** Heatmap displaying the top 5 characteristic genes for each cluster of the UMAP in **A**. Please also see Figure S5.

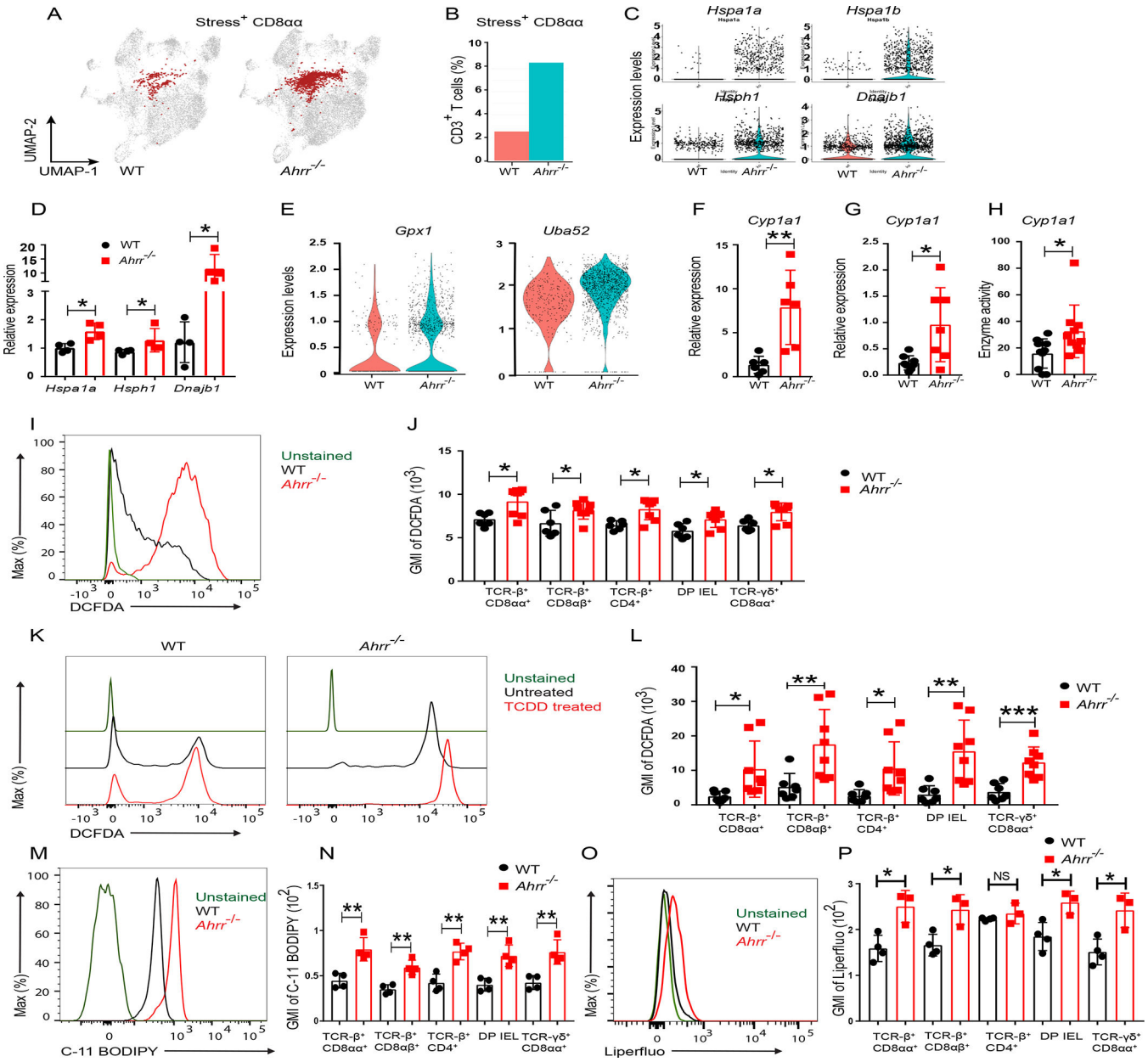

Figure 4. *Ahrr* deficiency induces oxidative stress in IEL.

(A) UMAP plot of stress response$^+$ CD8αα$^+$ IEL and **(B)** frequency of stress response$^+$ CD8αα out of CD3$^+$ T cells in WT and *Ahrr*$^{-/-}$ mice. **(C)** Differential expression of *Hspa1a, Hspa1b, Hsph1* and *Dnajb1* transcripts in stress response$^+$ CD8αα$^+$ from WT and *Ahrr*$^{-/-}$ mice. **(D)** Q-PCR analysis of stress response genes in CD8αα$^+$ IEL from WT and *Ahrr*$^{-/-}$ mice. **(E)** Violin plot depicting the expression of *Gpx1* and *Uba52* in stress response$^+$ CD8αα$^+$ IEL from WT and *Ahrr*$^{-/-}$ mice. **(F)** *CYP1A1* expression in ileal tissues of WT and *Ahrr*$^{-/-}$ mice analyzed by qPCR. **(G)** Relative expression of *CYP1A1* in IEL from WT and *Ahrr*$^{-/-}$ mice. **(H)** *CYP1A1* enzymatic activity in IEL from WT and *Ahrr*$^{-/-}$ mice upon stimulation with TCDD. **(I, J)** DCFDA staining of IEL from WT and *Ahrr*$^{-/-}$ mice: representative flow cytometry plots histogram of TCR-β$^+$ CD8αα$^+$ cells **(I)** and GMI

of DCFDA in different IEL subsets **(J)**. **(K, L)** DCFDA staining of WT and *Ahrr*$^{-/-}$ IEL upon TCDD stimulation: representative flow cytometry plots histograms TCR-β^{+} CD8αα^{+} cells **(K)** and quantification in different IEL subsets **(L)**. **(M, N)** C-11 BODIPY staining of WT and *Ahrr*$^{-/-}$ IEL: representative histograms of TCR-β^{+} CD8αα^{+} cells **(M)** and quantification in different IEL subsets **(N)**. Liperflou staining of WT and *Ahrr*$^{-/-}$ IEL: representative histograms of TCR-β^{+} CD8αα^{+} cells **(O)** and quantification in different IEL subsets **(P)**. Data are pool or representative of 2 individual experiments. Statistical significance was determined by Mann-Whitney test. *P<0.05, **P<0.01, ***P<0.001. Please also see Figure S6.

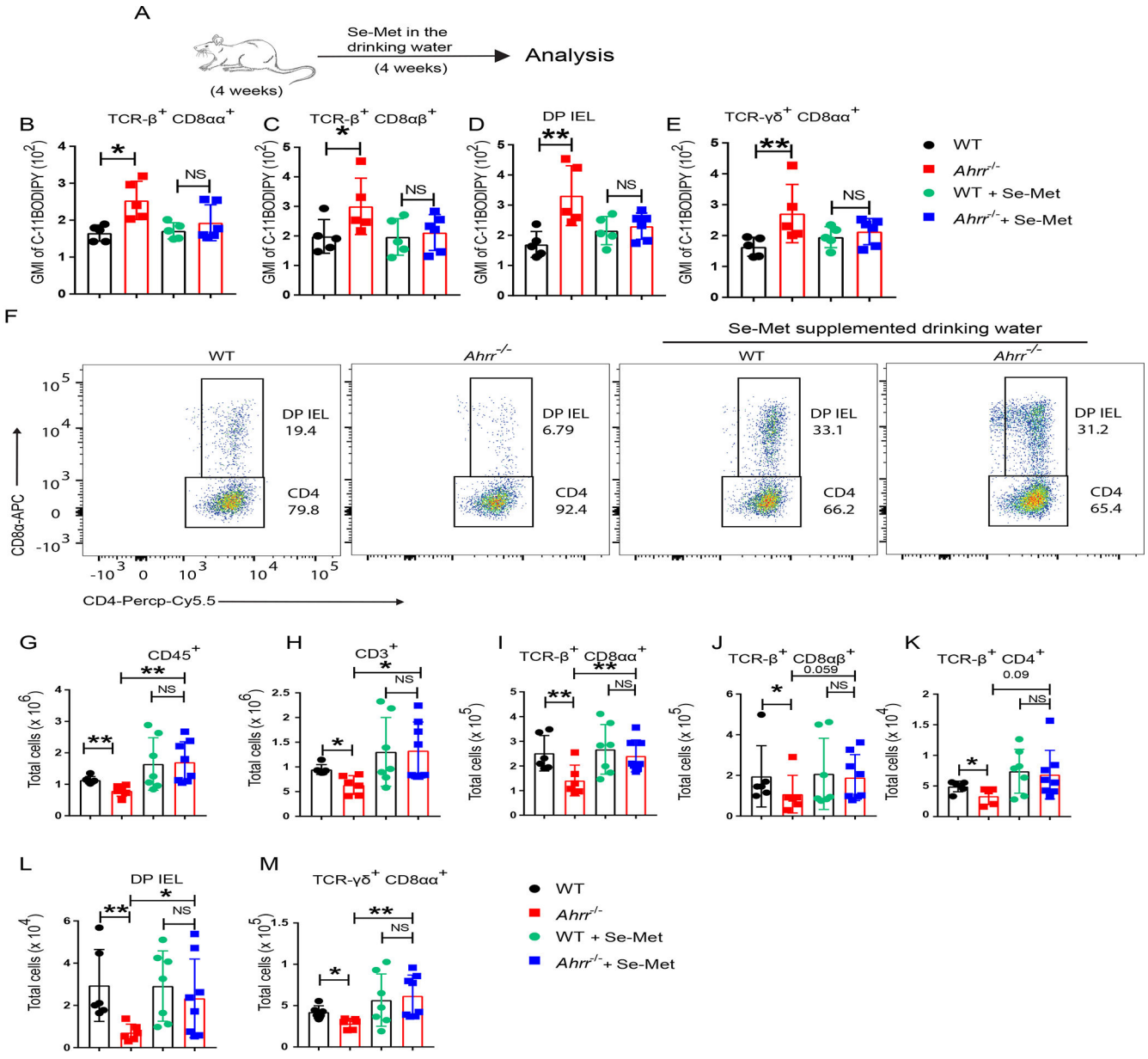

Figure 5. Dietary selenium supplementation rescues IEL loss in *Ahrr*$^{-/-}$ mice.

(A) WT and *Ahrr*$^{-/-}$ mice were treated with selenium supplemented drinking water (2mg/l) for 4 weeks and then IELs were stained for C-11 BODIPY. **(B-E)** GMI of C-11 BODIPY in different IEL populations: TCR-β$^+$ CD8αα$^+$ **(B)**; TCR-β$^+$ CD8 αβ$^+$ **(C)**; DP IEL **(D)**; and γδ IEL **(E)**. **(F)** Representative flow cytometry plots plots showing the DP IEL in WT and *Ahrr*$^{-/-}$ mice with and without dietary selenium supplementation. **(G-M)** Numbers of small intestinal CD45$^+$ IEL **(G)**, T cells in small intestinal epithelium **(H)**; TCR-β$^+$ CD8αα$^+$ IEL **(I)**, TCR-β$^+$ CD8αβ$^+$ IEL **(J)**; TCR-β$^+$ CD4$^+$ IEL **(K)**; DP-IEL **(L)**; and TCR-γδ$^+$ CD8αα$^+$ IEL **(M)**, of WT and *Ahrr*$^{-/-}$ mice with and without selenium supplementation. Each dot represents an individual mouse. Data are pool or representative of 2 individual experiments. Statistical significance was determined by Mann-Whitney test. *P<0.05, **P<0.01, ***P<0.001.

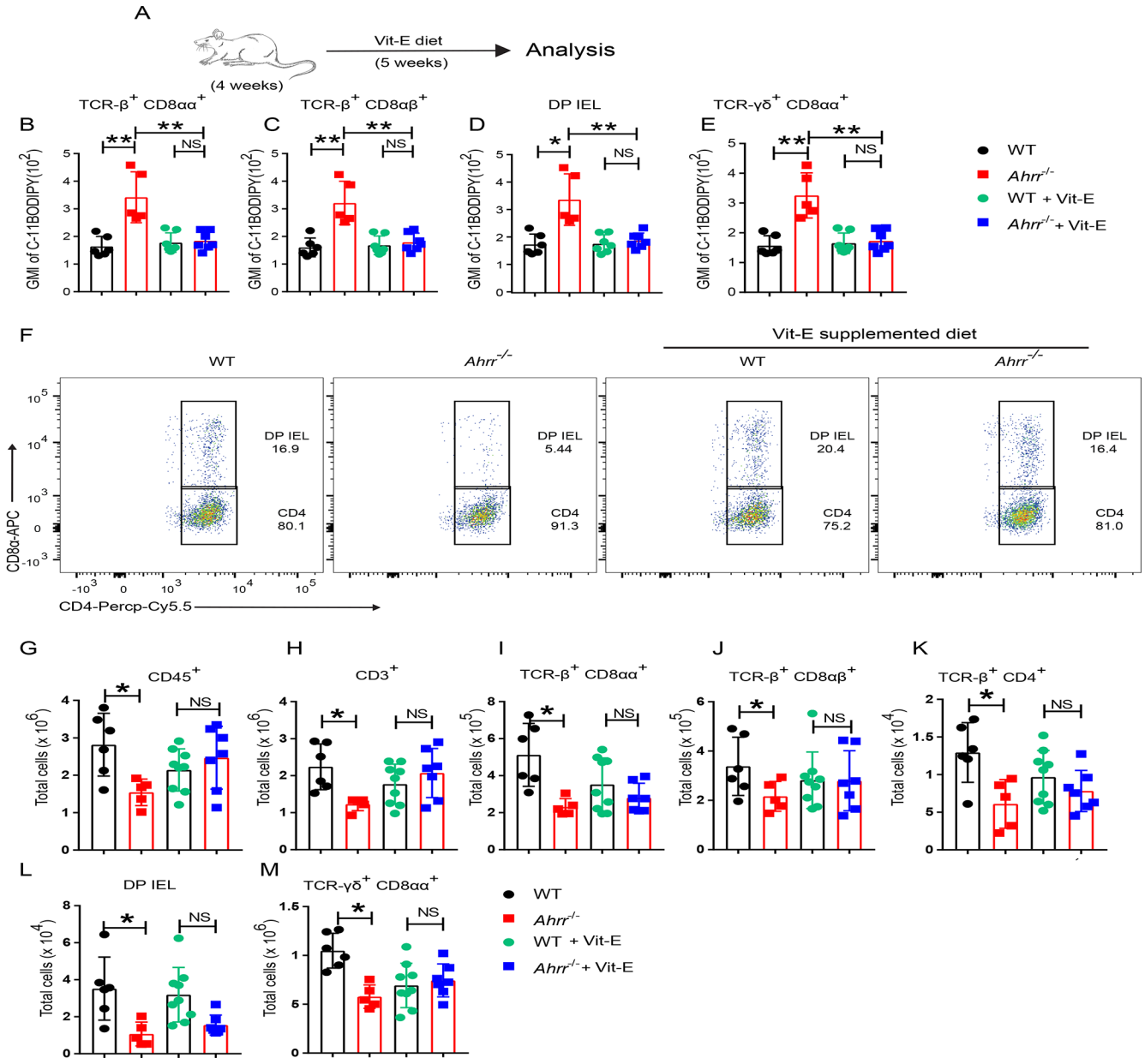

Figure 6. Dietary supplementation with Vit-E restores IEL in *Ahrr*$^{-/-}$ mice.

(A) WT and *Ahrr*$^{-/-}$ mice were fed a Vit-E rich diet for 5 weeks; IELs were stained for C-11 BODIPY. **(B-E)** GMI of C-11 BODIPY in different IEL populations: TCR-β$^+$ CD8αα$^+$ **(B)**; TCR-β$^+$ CD8 αβ$^+$ **(C)**; DP IEL **(D)**; and γδ IEL **(E)**. **(F)** Representative flow cytometry plots plots showing DP IEL in WT and *Ahrr*$^{-/-}$ mice with and without dietary Vit-E supplementation. **(G-M)** Numbers of small intestinal CD45$^+$ IEL **(G)**, T cells in the small intestinal epithelium **(H)**; TCR-β$^+$ CD8αα$^+$ IEL **(I);** TCR-β$^+$ CD8αβ$^+$ IEL **(J)**; TCR-β$^+$ CD4$^+$ IEL **(K)**; DP-IEL **(L)**; and TCR-γδ$^+$ CD8αα$^+$ IEL **(M)**, in WT and *Ahrr*$^{-/-}$ mice with and without Vit-E supplementation. Each dot represents an individual mouse. Data are pool or representative of 2 individual experiments. Statistical significance was determined by Mann-Whitney test. *P<0.05, **P<0.01, ***P<0.001.

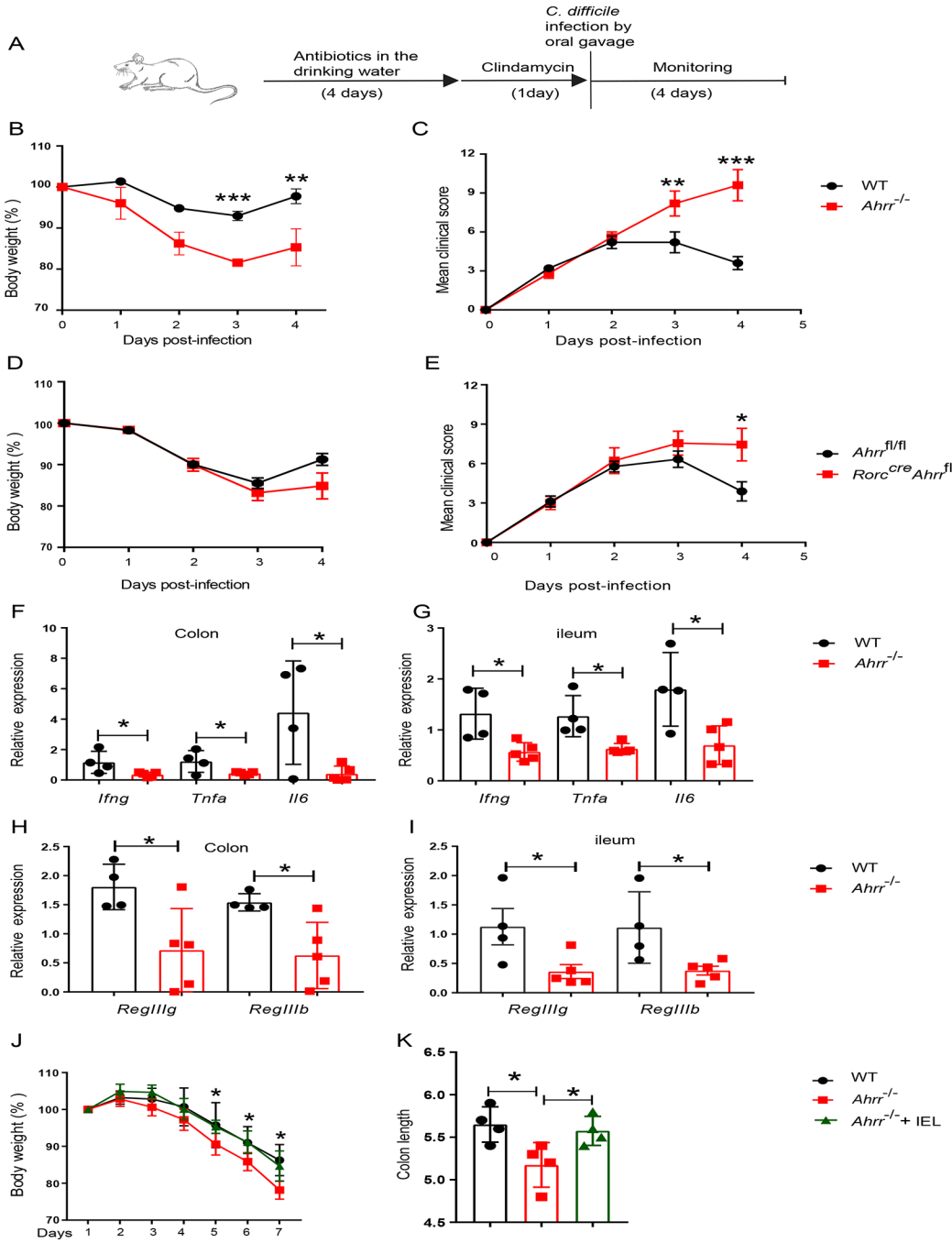

Figure 7. *Ahrr* deficiency augments susceptibility to intestinal pathology.

(A) Schematic of *C. difficile* infection in WT and *Ahrr*$^{-/-}$ mice or *Ahrr*$^{fl/fl}$ and Rorc^{cre} *Ahrr*$^{fl/fl}$ mice. **(B)** Body weight and **c**, clinical score in WT and *Ahrr*$^{-/-}$ mice. **(D)** Body weight and **(E)**, clinical score in *Ahrr*$^{fl/fl}$ and Rorc^{cre} *Ahrr*$^{fl/fl}$ mice. **(F-I)** Expression of *Ifng, Tnfa, Il6, RegIIIg* and *RegIIIb* in colonic and ileal tissues of WT and *Ahrr*$^{-/-}$ mice upon infection with *C. difficile*. **(J, K)** *Ahrr*$^{-/-}$ mice were reconstituted with WT IEL and, after 3 days, were challenged with 3% DSS for 7 days. **(J)** % of body weight variation and **(K)** colon length at day 7 in WT, *Ahrr*$^{-/-}$ and *Ahrr*$^{-/-}$ mice reconstituted

with WT IEL. Each dot represents an individual mouse. Data are pooled or representative of 2 individual experiments. Statistical significance was determined by Mann-Whitney test. *P<0.05, **P<0.01, ***P<0.001. Please also see Figure S7.

Key resources table

REAGENT or RESOURCE	SOURCE	IDENTIFIER
Antibodies		
anti-mouse CD45-APC-Cy7	Biolegend	Cat#103116; RRID: AB_312981
anti- mouse CD45-AF700	Biolegend	Cat#103128; RRID: AB_493715
anti- mouse CD45.1-PE-Cy7	Biolegend	Cat#110730; RRID: AB_1134168
anti- mouse CD45.2-APC-Cy7	Biolegend	Cat#109824; RRID: AB_830789
anti- mouse CD3 PACB	Biolegend	Cat#100334; RRID: AB_2028475
anti- mouse CD3 PE/Cy7	Biolegend	Cat#100320; RRID: AB_312685
anti- mouse CD3 APC/Cy7	Biolegend	Cat#100222; RRID: AB_2242784
anti- mouse CD4-PerCP-Cy5.5	Biolegend	Cat#100434; RRID: AB_893324
anti- mouse CD4- PE/Cy7	Biolegend	Cat# 100422; RRID: AB_312707
anti-CD8α-APC	Biolegend	Cat#100712; RRID: AB_ 312751
anti-CD8β-FITC	Biolegend	Cat#126606; RRID: AB_ 961295
anti-CD8β-PerCP-Cy5.5	Biolegend	Cat#126610; RRID: AB_ 2260149
anti-TCR-γδ-PE	Biolegend	Cat#118108; RRID: AB_ 313832
anti-TCR-γδ-BV421	Biolegend	Cat#118119; RRID: AB_ 2562566
anti-CD3-PerCP-Cy5.5	Biolegend	Cat#100328; RRID: AB_ 893318
anti-CD5-PerCP-Cy5.5	Biolegend	Cat#100624; RRID: AB_ 2563433
anti-CD19-PerCP-Cy5.5	Biolegend	Cat#115534; RRID: AB_ 2072925
anti-RORγT-APC	Invitrogen	Cat#17-6988-82; RRID: AB_10609207
anti-RORγT-PE	Invitrogen	Cat#12-6988-82; RRID: AB_1834470
anti-GATA3-AF488	BD	Cat#560077; RRID: AB_1645303
anti-EOMES-PE	Invitrogen	Cat#12-4875-82; RRID: AB_1603275
anti-FoxP3-AF647	Biolegend	Cat#124608; RRID: AB_ 1089115
anti-CD69-BV605	Biolegend	Cat#104529; RRID: AB_ 11203710
anti-CCR9- PE/Cy7	Biolegend	Cat#128712; RRID: AB_ 10933082
anti-CD103-Biotin	Invitrogen	Cat#13-1031-85; RRID: AB_ 466553
anti-NKp46-Biotin	Biolegend	Cat# 137616; RRID: AB_ 11218796
anti-CCR6-BV421	Biolegend	Cat# 129818; RRID: AB_ 11219003
anti-CD90.2-APC	Biolegend	Cat# 129818; RRID: AB_ 313183
anti-IL-17A-FITC	Biolegend	Cat# 506908; RRID: AB_ 536010
anti-IL-22-PE	Invitrogen	Cat# 12-7221-82; RRID: AB_ 10597428
anti-IFN-γ-PE	Biolegend	Cat# 505808; RRID: AB_ 315402
Biological samples		
Intestinal tissue from healthy and IBD patients	Washington University in St. Louis	N/A
Bacteria		
C. difficile	Colonna Lab	VPI 10463
Chemicals, peptides, and recombinant proteins		

REAGENT or RESOURCE	SOURCE	IDENTIFIER
Mouse IL-23	R&D	Cat#1887-ML
Mouse IL-2 supernatant	Colonna Lab	N/A
Mouse IL-4 supernatant	Colonna Lab	N/A
Collagenase from Clostridium histolyticum	Sigma	Cat#C5138
Critical commercial assays		
Foxp3 transcription factor staining Buffer set	eBioscience	Cat#00-5523-00
BD Cytofix/Cytoperm Plus	BD Biosciences	Cat#555028
LS Columns	Miltenyi Biotec	Cat#130-042-401
CD45 MicroBeads, mouse	Miltenyi Biotec	Cat#130-052-301
Pan T Cell Isolation Kit II, mouse	Miltenyi Biotec	Cat#130-095-130
RNeasy Plus Micro Kit	QIAGEN	Cat#74034
Deposited data		
Single cell RNAseq data	This paper	GSE199960
Experimental models: Organisms/strains		
Mouse: *Ahrr*$^{fl/fl}$, *Ahrr*$^{-/-}$	This study	N/A
Mouse: *Rorc*^{cre}	Tumanov lab	N/A
Mouse:CD45.1	Jackson lab	JAX:002014
Mouse: CD45.1/2	This study	N/A
Oligonucleotides		**Sequence**
Reg-IIIb-Fwd	Integrated DNA Technologies	TCCCAGGCTTATGGCTCCTA
Reg-IIIb-Rev	Integrated DNA Technologies	GCAGGCCAGTTCTGCATCA
Reg-IIIg-Fwd	Integrated DNA Technologies	CATCAACTGGGAGACGAATCC
Reg-IIIg-Rev	Integrated DNA Technologies	CAGAAATCCTGAGGCTCTTGACA
Ahrr-Fwd	Integrated DNA Technologies	CTGCCCCGGGATCAAAGATG
Ahrr-Rev	Integrated DNA Technologies	CTCTGTATTGAGGCGGTCCC
Cyp1a1- Fwd	Integrated DNA Technologies	GACATTTGAGAAGGGCCACAT
Cyp1a1-Rev	Integrated DNA Technologies	TCCTGGATCTTTCTCTGTACCC
Il6- Fwd	Integrated DNA Technologies	GAGGATACCACTCCCAACAGACC
Il6- Rev	Integrated DNA Technologies	AAGTGCATCATCGTTGTTCATACA
Ifng- Fwd	Integrated DNA Technologies	AGGAACTGGCAAAAGGATGGT
Ifng- Rev	Integrated DNA Technologies	ACCTGTGGGTTGTTGACCTC
Tnfa- Fwd	Integrated DNA Technologies	CATCTTCTCAAAATTCGAGTGACAA
Tnfα- Rev	Integrated DNA Technologies	TGGGAGTAGACAAGGTACAACCC
Hsph1 -Fwd	Integrated DNA Technologies	TGCAGCACTATGCCAAGATTG
Hsph1 -Rev	Integrated DNA Technologies	TTCTCAACCTTCTTCATTTCTGATTC
Dnajb1-Fwd	Integrated DNA Technologies	TTCGACCGCTATGGAGAGGAA
Dnajb1-Rev	Integrated DNA Technologies	CACCGAAGAACTCAGCAAACA
Hspa1a-Fwd	Integrated DNA Technologies	ATGGACAAGGCGCAGATCC

REAGENT or RESOURCE	SOURCE	IDENTIFIER
Hspa1a-Rev	Integrated DNA Technologies	CTCCGACTTGTCCCCCAT
Software and algorithms		
FlowJo	Tree Star	https://www.flowjo.com/
Prism	Graphpad	https://www.graphpad.com/
Endnote	Endnote	https://endnote.com/
Seurat	R	https://satijalab.org/seurat/
Biorender	Biorender	https://biorender.com/